Science of the Total Environment 666 (2019) 540–558

Contents lists available at ScienceDirect

Science of the Total Environment

journal homepage: www.elsevier.com/locate/scitotenv

Source apportionment of ambient fine and coarse particulate matter polycyclic aromatic hydrocarbons at the Bertha Ganter-Fort McKay community site in the Oil Sands Region of Alberta, Canada

Matthew S. Landis [a,*], William B. Studabaker [b], J. Patrick Pancras [c], Joseph R. Graney [d], Emily M. White [e], Eric S. Edgerton [f]

[a] Integrated Atmospheric Solutions, LLC., Cary, NC, USA
[b] Tobacco Road Collaborative, LLC, Raleigh, NC, USA
[c] Pancras Consulting, Cary, NC, USA
[d] Geological Sciences and Environmental Studies, Binghamton University, Binghamton, NY, USA
[e] Maed Consulting, Pittsboro, NC, USA
[f] Atmospheric Research & Analysis, Inc., Cary, NC, USA

HIGHLIGHTS

- Ambient PM PAH source apportionment study conducted in Athabasca Oil Sands Region.
- Receptor modeling elucidated and quantified significant contributing PM sources.
- C1- and C2-alkyl PAHs and dibenzothiophenes utilized as tracer species.
- One pyrogenic $PM_{2.5}$ source factor contributed 78% of the measured ΣPAH.
- One organic aerosol $PM_{10-2.5}$ source factor contributed 86% of the measured ΣPAH.

GRAPHICAL ABSTRACT

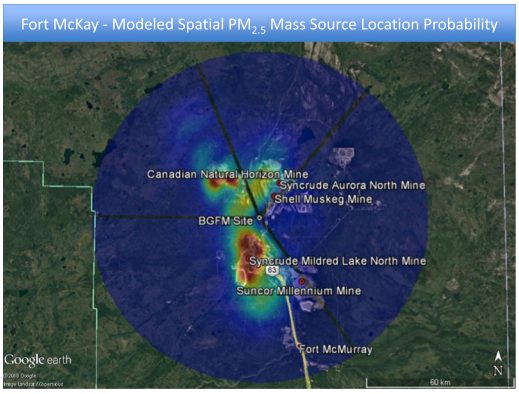

ARTICLE INFO

Article history:
Received 1 November 2018
Received in revised form 28 January 2019
Accepted 8 February 2019
Available online 10 February 2019

Editor: Kelly Roland Munkittrick

Keywords:
Fugitive dust
Biomass combustion
$PM_{2.5}$
PM_{10}
PAHs, PACs

ABSTRACT

A comprehensive filter-based particulate matter polycyclic aromatic hydrocarbon (PAH) source apportionment study was conducted at the Wood Buffalo Environmental Association Bertha Ganter-Fort McKay (BGFM) community monitoring station from 2014 to 2015 to quantify ambient concentrations and identify major sources. The BGFM station is located in close proximity to several surface oil sands production facilities and was previously found to be impacted by their air emissions. 24-hour integrated $PM_{2.5}$ and $PM_{10-2.5}$ samples were collected on a 1-in-3-day schedule yielding 108 complete organic/inorganic filter sets for source apportionment modeling. During the study period $PM_{2.5}$ averaged 8.6 ± 11.8 μg m^{-3} (mean ± standard deviation), and $PM_{10-2.5}$ averaged 8.5 ± 9.5 μg m^{-3}. Wind regression analysis indicated that the oil sands production facilities were significant sources of $PM_{2.5}$ mass and black carbon (BC), and that wildland fires were a significant source of the highest $PM_{2.5}$ (>10 μg m^{-3}) and BC events. A six-factor positive matrix factorization (PMF) model solution explained 95% of the measured $PM_{2.5}$ and 78% of the measured ΣPAH. Five sources significantly contributed to $PM_{2.5}$ including: Biomass Combustion (3.57 μg m^{-3}; 40%); Fugitive Dust (1.86 μg m^{-3}; 28%); Upgrader Stack Emissions (1.44 μg m^{-3}; 21%); Petrogenic PAH (1.20 μg m^{-3}; 18%); and Transported Aerosol (0.43 μg m^{-3} and 6%).

* Corresponding author.
E-mail address: mlandis@atmospheric-solutions.com (M.S. Landis).

https://doi.org/10.1016/j.scitotenv.2019.02.126

However, the analysis indicated that only the pyrogenic PAH source factor significantly contributed (78%) to the measured ΣPAH. A five-factor PMF model dominated by fugitive dust sources explained 98% of $PM_{10-2.5}$ mass and 86% of the ΣPAH. The predominant sources of $PM_{10-2.5}$ mass were (i) Haul Road Dust (4.82 μg m^{-3}; 53%), (ii) Mixed Fugitive Dust (2.89 μg m^{-3}; 32%), (iii) Fugitive Oil Sand (0.88 μg m^{-3}; 10%), Mobile Sources (0.23 μg m^{-3}; 2%), and Organic Aerosol (0.06 μg m^{-3}; 1%). Only the Organic Aerosol source significantly contributed (86%) to the measured ΣPAH.

1. Introduction

The Athabasca Oil Sands Region (AOSR) in Northern Alberta, Canada is a large oil producing region with recoverable reserves of 165 billion barrels (Alberta Energy Regulator, 2017) and an average production rate of 2.5 million barrels per day in 2016 (Alberta Energy, 2017). What sets this region apart from other oil producing regions is that the majority (55% in 2014 and 2015) of bitumen production in the AOSR was recovered in open pit surface shovel and heavy hauler mining operations, a substantial portion of the produced bitumen is upgraded at regional facilities from heavy sour to light sweet synthetic crude, and upgrading byproducts (e.g., petroleum coke, sulfur) are consolidated and stored on site in large above ground stock piles (Foster et al., 2019). Emissions from bitumen mining, heavy hauling operations, upgrading, and stockpiling of byproducts have all been identified as sources of ambient particulate matter (PM) in surrounding regional communities (Landis et al., 2017; Phillips-Smith et al., 2017). Mining operations in the AOSR utilize large fleets of some of the world's largest trucks such as the Caterpillar CAT 797B heavy hauler with a 345 Mt. capacity burning ultra-low sulfur diesel fuels (<15 ppm; Wang et al., 2016). Atmospheric emissions from shovel and mine heavy hauler fleet operations include emissions from raw oil sand and haul road fugitive (wind-blown) dust as well as diesel engine combustion exhaust (Landis et al., 2012; Landis et al., 2019; Wang et al., 2015; Wang et al., 2016).

The emission of polycyclic aromatic hydrocarbons (PAHs) from bitumen production activities and subsequent atmospheric deposition and accumulation in the terrestrial and aquatic ecosystems has recently been a focal point for researchers in the AOSR due to their potential for human and ecological toxicity (Kelly et al., 2009; Kurek et al., 2013; Bari et al., 2014; Schindler, 2014; Ahad et al., 2015; Schuster et al., 2015; Lundin et al., 2015; Birks et al., 2017; Boutin and Carpenter, 2017; Droppo et al., 2018; Fernie et al., 2018; Harner et al., 2018). Recent studies have begun to focus on ambient PAH concentrations in local communities (Hsu et al., 2015; Wnorowski, 2017; Wentworth et al., 2018), and the origins of PAHs in environmental samples and strategies for the mitigation of environmental impacts in the AOSR (Ahad et al., 2015; Jautzy et al., 2015; Korosi et al., 2016; Zhang et al., 2016; Manzano et al., 2017). However, there have been no efforts to identify the sources of ambient PAHs measured in communities that are in close proximity to oil sands production operations.

PAHs are formed from a variety of natural and anthropogenic processes and the relative abundances of individual species in an air emission (profile) can vary by source. Attribution of PAHs in environmental samples to one or more sources depends on an accurate profile of each source that may contribute to deposition at the sampling location, and on the identification of specific molecular markers or indices that individually or collectively serve as a "fingerprint" for each source (Stogiannidis and Laane, 2015). This approach has been used for source attribution of PAHs in environmental samples from the AOSR (Wang et al., 2014). In addition, source attribution tools such as diagnostic ratios, double ratio plots, and principal components analysis have been used for elucidation of source inputs in atmospheric samples (Ravindra et al., 2008; Stogiannidis and Laane, 2015). Care must be used in the application of such tools, as it is often assumed that profile characteristics are unique and unchanged during transport from source to receptor, whereas factors such as vapor-particle partitioning, photochemical reactions, and air-water exchange may significantly alter the profile characteristics (Galarneau, 2008). Polycyclic aromatic compounds (PACs) beyond conventional PAH species (such as alkylated-PAHs, dibenzothiophenes, and retene) have recently been identified as useful tracer species for various oil sands related sources in the AOSR (Jautzy et al., 2013; Harner et al., 2018; Landis et al., 2019).

This paper presents results from a study designed to (i) measure ambient PAH concentrations in aerosol, semi-volatile, and volatile phase ($PM_{2.5}$, $PM_{10-2.5}$, total suspended particulate) concentrations in Fort McKay, Alberta, and (ii) use a multivariate statistical receptor modeling approach to identify source contributions for observed PAHs by also incorporating elemental and PAC tracer species. Fort McKay is a centrally located community in the AOSR that has been shown to be impacted by emissions from nearby surface oil sand mining and bitumen upgrading operations as well as by emissions from wildland fires (Landis et al., 2012; Landis et al., 2017; Phillips-Smith et al., 2017; Wentworth et al., 2018).

2. Methods

2.1. Sampling site

The Wood Buffalo Environmental Association (WBEA) Bertha Ganter-Fort McKay (BGFM) ambient air monitoring station (57°11′ 21.70″ N; −111°38′26.06″ W) is located in the Fort McKay First Nation and Metis community, Alberta, Canada. This monitoring site was originally established in 1983 as an Alberta Environment station and was later incorporated into the WBEA network, moved to its current location and upgraded with additional monitoring capabilities in 1997. The BGFM monitoring site is close to several ongoing surface oil sand production operations including oil sand mines and bitumen upgrading operations (Fig. 1), and provides real-time ambient air quality information, such as the Canadian Air Quality Health Index (AQHI), to the community (https://wbea.org).

2.2. Routine WBEA measurements

In addition to the study-specific measurements discussed in subsequent sections, data from WBEA's ambient monitoring program were incorporated into this study, including continuous 5 min integrated (i) $PM_{2.5}$ mass measured using ThermoScientific (Franklin, MA) Model 5030 Synchronized Hybrid Ambient Real-time Particulate Monitor (SHARP), (ii) nitrogen oxide (NO), nitrogen dioxide (NO_2), and total oxides of nitrogen (NOx) measured using a ThermoScientific Model 42i chemiluminescence analyzer, (iii) sulfur dioxide (SO_2) measured using a ThermoScientific Model 43i pulsed fluorescence analyzer, (iv) total reduced sulfur (TRS) measured using a ThermoScientific Model 43i coupled with a CD Nova Ltd. (Surrey, BC) Model CDN101 high temperature thermal oxidizer, (v) total hydrocarbons (THC), non-methane hydrocarbons (NMHC), and methane (CH_4) measured using a ThermoScientific Model 55i gas chromatography flame ionization detector (FID) instrument, (vi) black carbon (BC) measured using a Magee Scientific (Berkeley, CA) Model AE-22 Aethalometer (Appendix A), (vii) ozone measured using a ThermoScientific Model 49i UV absorption analyzer, and (viii) ammonia (NH_3) measured using a

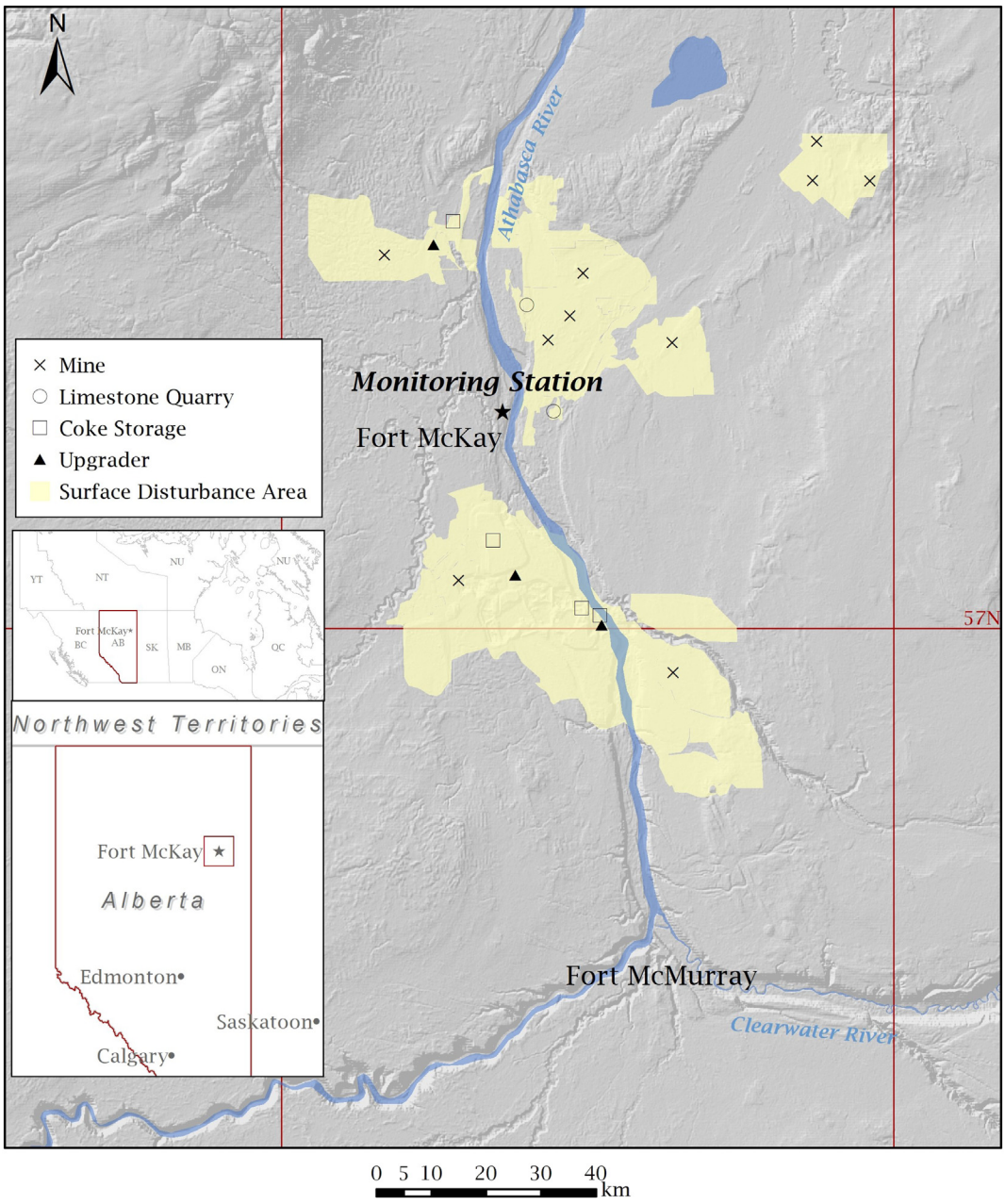

Fig. 1. Map Depicting the Location of the WBEA Betha Ganter - Fort McKay Ambient Monitoring Station and the Surrounding Major Surface Oil Sand Production Facilities Operating during the 2014–2015 Study Period.

ThermoScientific Model 17i chemiluminescence analyzer (WBEA, 2011).

2.3. Collection of ambient particulate matter for PAHs & PACs

Tisch Environmental (Cleves, OH) Model TE-6070D-BL and Model TE-6070D-2.5-HVS 1.13 m^3 min^{-1} samplers were installed at the BGFM monitoring site for PM_{10} and $PM_{2.5}$ sampling, respectively. Twenty-four-hour integrated samples were collected from October 20, 2014 to October 31, 2015 on a one-in-three-day schedule coincident with the Environment Canada National Air Pollution Surveillance Program (NAPS) sampling schedule. Pre-combusted 8″ x 10″ quartz fiber filters (Pall, Port Washington, NY) were utilized for sampling, and field blanks for $PM_{2.5}$ and PM_{10} were collected at least monthly.

A Tisch Model TE-1000 High Volume Plus sampler was used to collect total suspended particulates (TSP) onto pre-combusted 90 mm quartz filters (Advantec MFS, Dublin, CA). The High Volume Plus sampler was equipped with a backup chamber for the insertion of a combination polyurethane foam (PUF) and hydrophobic crosslinked adsorbent polystyrene copolymer resin (XAD) for the collection of semi-volatile/volatile PAHs & PACs. The use of the PUF sampler in this study was to investigate the presence of PAH aerosols greater than PM_{10} by comparing the TSP and collocated PM_{10} Tisch sampler results. Since this was an exploratory portion of the study, these samples were only collected on a 1-in-24-day schedule. Quartz TSP/PUF/XAD samplers were prepared by Eastern Research Group (ERG; Morrisville, NC, USA), according to U.S. EPA method TO-13A (U.S. Environmental Protection Agency, 1999). Field blanks for TSP/PUF/XAD were collected in October and November 2014, and August and October 2015.

2.4. Quartz filter and PUF/XAD sample extraction and analysis

A detailed description of the Quartz Filter and PUF/XAD Sample Extraction and Analysis methods can be found in Appendix B. Briefly,

TSP filters and PUF/XAD media were extracted separately according to U.S. EPA Method TO-13A (U.S. Environmental Protection Agency, 1999) to discriminate between particle-bound and vapor-phase PAHs and PACs using a Dionex (Sunnyvale, CA) Model 300 accelerated solvent extractor (ASE) with 20 mL of hexane/acetone (70/30) at 100 °C and 1200 PSI. Samples were then concentrated by blowing down under an ultra-high purity (UHP) nitrogen gas stream to 1 mL, and the PUF/XAD sample extracts were cleaned with silica gel solid phase extraction (SPE) cartridges prior to analysis.

Analysis of filter and PUF/XAD extracts for PAHs and PACs were performed on a LECO (St. Joseph, MI) Pegasus 4D gas chromatograph with time-of-flight mass spectral detection (GC-TOF-MS) as described in Studabaker et al. (2017). The GC-TOF-MS was calibrated using standards up to 250 ng mL^{-1} (9 levels) for PACs and 2500 ng mL^{-1} for PAHs (12 levels). PACs refer to C1 and C2 alkyl PAHs, dibenzothiophene, and the alkyl dibenzothiophenes. Alkyl PAHs are assigned to groups and named based on the level of alkylation of the parent PAH or a member of a group of structural isomers. Thus, methylfluoranthenes and methylpyrenes are included in the C1-fluoranthenes, while dimethylphenanthrenes and ethylphenanthrenes are included in the C2-phenanthrenes (Wang and Fingas, 2003). For analytical reasons (Studabaker et al., 2017) we limited our investigation to dibenzothiophene and C1 and C2 PACs. Retene (a C4-phenanthrene) was also included because it is a tracer species for softwood combustion (Ramdahl, 1983; Schauer et al., 1996; Simoneit, 2002). Study specific MDLs and the percentage of samples above MDL, by analyte and particulate matter size fraction, are summarized in Appendix Table C.1.

2.5. Collection and analysis of ambient particulate matter for elemental determination

Twenty-four-hour ambient PM samples were collected and analyzed for mass and elemental determination on the same NAPS schedule as the Tisch samplers following procedures described in Landis et al. (2017) to provide relevant tracer species information. Briefly, samples were collected onto Teflon filters using a ThermoScientific Model 2025D Sequential Dichotomous air sampler (a U.S. EPA designated Federal Equivalent Method for $PM_{2.5}$). Measurement Technologies Laboratories (MTL; Minneapolis, MN) 47 mm Teflon membrane filters with Teflon support rings were utilized for this study. Atmospheric Research & Analysis, Inc. (ARA, Morrisville, NC, USA) pre- and post-weighed the filters in a Class 1000 clean room using a Mettler Toledo (Columbus, OH) Model UMX2 microbalance equipped with an MTL Model AH225–6 robotic auto-handler that performed five replicate weighings of each filter.

The relationship between the $PM_{2.5}$ mass measurements derived from the WBEA routine semi-continuous SHARP instrument and the study specific 24-hour integrated dichotomous sampler filter for the study period is presented in Appendix Fig. D.1. The slope of the linear regression line was 0.988 and the coefficient of determination was 0.924. On average, the two samplers provided highly correlated results with an absolute median concentration difference of 0.9 μg m^{-3}, and an absolute median percent difference (AMPD) of 15%. Relative frequency histograms of the fine and coarse particulate matter concentrations are presented in Appendix Fig. D.2 showing (i) skewed right log-normal particulate matter mass distributions, and (ii) two $PM_{2.5}$ mass outliers with the year's highest two concentration values of 87.3 and 78.1 μg m^{-3} with the coincident $PM_{10-2.5}$ mass samples not reflecting similar dramatic increases. These two sampling days (June 29 & July 11, 2015) represent impacts from local wildland fire smoke that was confirmed by concurrent BC, NH_3, and TRS measurements.

The dichotomous sampler filters were microwave digested and analyzed for a suite of 42 elements (Al, Sb, As, Ba, Be, Bi, Cd, Ca, Ce, Cs, Cr, Co, Cu, Fe, La, Pb, Li, Mg, Mn, Mo, Nd, Ni, Nb, P, Pt, K, Pr, Rb, Sm, Se, Si, Na, Sr, Ta, Tl, Th, Sn, Ti, W, U, V, Zn) by ARA as described in Landis et al. (2017). Briefly, filters were microwave-extracted in a mixture of ultra-pure H_2O_2, HF, and HNO_3 with heating to 180 °C for 40 min. After cooling, American Society of Testing and Materials (ASTM) Type I ultrapure (18.2 MΩ·cm) water was added to each vessel to bring the extract up to a final volume of 15 mL. The sample extracts were then analyzed using a Perkin-Elmer (Waltham, MA) Model 9000 Elan-II dynamic reaction cell inductively coupled plasma mass spectrometer (DRC-ICPMS). Instrument drift and suppression, or enhancement of instrument response caused by the sample matrix, was corrected by internal standardization (Edgerton et al., 2012). The average field blank loading for each analyte was used to blank-correct samples for mass and trace elements. Study specific MDLs and the percentage of samples above MDL, by analyte and particulate matter size fraction, are summarized in Appendix Table C.2.

2.6. Source apportionment modeling

The EPA's multivariate Positive Matrix Factorization (PMF) v5.1 receptor model (U.S. EPA, 2014) was applied on the size-segregated datasets ($PM_{2.5}$ and $PM_{10-2.5}$) for mass apportionment. PMF is described in greater detail in Paatero and Tapper (1993) and Paatero (1997). Briefly, the EPA implementation of PMF uses a graphical user interface that has been developed on the PMF model, and the general mixed linear model is solved using the Multilinear Engine-2 program (Paatero, 1999). EPA PMF operates in a robust mode, meaning outlier species concentrations are not allowed to overly influence the factor solutions. Additionally, the feature of individual weighting of each data point allows the model to calculate covariance in the receptor data matrix based on reliability of each chemical measurement.

A total of 13 particle bound PAH and PAC species, known to be stable on filter media based on volatility were selected for PMF modeling to prevent gas and particle phase partitioning of PAH and PAC species from influencing factor profiles including: Benz[*a*]anthracene, Chrysene, Benzo[*bj*]fluoranthene, Benzo[*k*]fluoranthene, Benzo[*e*]pyrene, Benzo[*a*]pyrene, Indeno[1,2,3-*cd*]pyrene, Dibenz[*a*,*h*]anthracene, Benzo[*g*,*h*,*i*]perylene, C1-Chrysene isomers, C1-Benzopyrenes/Benzofluoranthenes, C2-Chrysene isomers, and C2-Benzopyrenes/Benzofluoranthenes. Of the 42-inorganic species measured, Be, Sn, Bi, W, Th, Tl, and U were excluded due to their low observed concentrations, and Cu was excluded due to potential contamination from on-site carbon vane pump emissions (Pancras et al., 2013; Landis et al., 2017). Daily averaged BC measured at BGFM was also incorporated into the analysis within the PMF resolved factors. Measured PM mass was input in the model runs as a total variable in the $PM_{2.5}$ and $PM_{10-2.5}$ datasets.

All measured concentration data were retained for PMF analysis in this study with 'at or below detection' concentrations replaced by 1/2 of the MDL. Overall measurement error for each concentration data point was estimated from the respective GC-TOF-MS, LECO, and DRC-ICPMS MDL and duplicate analysis precision (U.S. EPA, 2014; Reff et al., 2007). Sampling error for the Tisch high volume and ThermoEnvironmental dichotomous samplers were estimated to be 10% and 5%, respectively, and was included in the overall error propagation equation. If the measured concentration was > MDL, then uncertainty was estimated using Eq. 1.

$$Uncertainty = \sqrt{\left(\frac{5}{6} \times MDL\right)^2 + (conc. \times analytical\ error)^2 + (conc. \times sampling\ error)^2} \quad (1)$$

Uncertainty was set as (5/6) × MDL if the measured concentration was ≤MDL.

Species selection relied on EPA PMF5.1 model-calculated signal-to-noise ratio, and analytes with a signal-to-noise ratio <1 were excluded from PMF modeling. Analytes with signal-to-noise ratio in the range

1–3 were set as "Weak". The PMF model, inflates the uncertainty of "Weak" species by three times, thereby letting species that are strongly associated with factors drive the solution. Based on signal-to-noise ratios Si, Cr, Ni, benzo(k)fluoranthene, benzo(a)pyrene, dibenz(a,h)anthracene, and C2-dibenzothiophenes were set as weak variables and the remaining species as strong variables. An extra modeling uncertainty of 5% was applied to all species to conservatively capture potential errors that were not initially considered in calculating measurement uncertainty. Two error estimation methods for analyzing factor analytic solutions were used to objectively evaluate the PMF model numerical solutions: (i) bootstrap analysis which captures random errors; and (ii) displacement analysis which deals with errors associated with factor rotational ambiguity (USEPA, 2014).

2.7. Wind regression analysis

Wind regression analysis was developed as a means of using semi-continuous (e.g., sub-hourly time resolution) meteorological and pollutant data to estimate the proportion of a given pollutant originating from a specific wind sector (sector apportionment). When trying to understand the local contributions of air pollution, visual tools can be used to illustrate the contributions from surrounding local sources. The sustained wind incidence method (SWIM; Vedantham et al., 2012) was applied to BGFM site 1 h averaged ambient monitoring and meteorological data. The SWIM model uses a kernel smoothing method to apportion high time resolution measurements into sectors based on surface meteorology at a receptor site (Vedantham et al., 2012). These sector constraints elucidated how local emissions from surrounding oil sand production operations contributed to the measured air pollutants at BGFM. The SWIM model includes the standard deviation of the wind direction, which was envisioned as an improvement upon the non-parametric wind regression method (Henry et al., 2009) by reducing the influence of a high frequency sector(s) and minimizing the impact of abrupt changes in wind direction (Vedantham et al., 2012). Additional details on smoothing functions, weighting procedures, and error estimation can be found in Vedantham et al. (2012) and Henry et al. (2009).

3. Results and discussion

3.1. Bertha Ganter-Fort McKay (BGFM) ambient monitoring results

Particulate matter mass was evaluated first to assess the representativeness of the 1-in-3-day sampling schedule to the annual concentrations at BGFM, as well as putting this study sampling period in context with routine observations in previous years. A summary of 24-hour integrated ambient air concentrations is presented in Table 1. The good agreement between the 1-in-3-day Teflon filter based $PM_{2.5}$ mass measurements (8.6 ± 11.8 μg m^{-3}; mean ± standard deviation) and the daily integrated SHARP instrument $PM_{2.5}$ mass measurements (8.1 ± 11.5 μg m^{-3}) suggests that the Dichotomous sampler captured a representative subset of the study period particulate matter sample day population. The average $PM_{2.5}$, $PM_{10-2.5}$ (8.5 ± 9.5 μg m^{-3}), BC (0.8 ± 1.2 μg m^{-3}), sulfur dioxide (1.1 ± 2.6 ppb), total hydrocarbon (1.9 ± 0.2 ppm), and methane (1.9 ± 0.2 ppm) concentrations are relatively low at BGFM. However, there are some relatively high concentration events that indicate significant impacts from natural wildland fire smoke emissions and local anthropogenic sources. For example, the maximum $PM_{2.5}$ concentrations reached 472 μg m^{-3}, BC reached 24.8 μg m^{-3}, and sulfur dioxide reached 52 ppb during the study sampling period. The only pollutant to exceed the Alberta Ambient Air Quality Objectives (AAAQO) or the Alberta Ambient Air Quality Guidelines (AAAQG) was $PM_{2.5}$ mass (Appendix Table C.3). Of the 101 hourly $PM_{2.5}$ AAAQG exceedances, 99 were associated with a known June 29–July 11, 2015 wildland fire smoke episode, and all 11 of the 24-hour $PM_{2.5}$ AAAQO exceedances were associated with the same smoke episode.

The long-term trends (1999–2015) of $PM_{2.5}$ and other gas phase pollutants (e.g., NO_X, SO_2, THC) at BGFM were presented and discussed in Landis et al. (2017) and Davidson and Spink (2018) in the context of increasing oil sand production and wildland fire activity over this period. Landis et al., 2017 reported that median long-term $PM_{2.5}$ concentration records did not indicate a significant trend, however, in four out of the last five years elevated wildland fire smoke impacted concentration outliers (2011, 2012, 2014, 2015) were observed. The impact of the statistical outliers was highlighted in a time series analysis of the annual mean $PM_{2.5}$ mass concentration trend from 1999 to 2015, which was found to be significantly increasing. The monthly geometric mean of hourly $PM_{2.5}$ concentrations at BGFM (1999–2017) are presented in Appendix Fig. D.3 with the study period highlighted. The months with exceptional wildland fire smoke impacts are clearly observable in the summers of 2011, 2012, 2014, 2015, and 2016, however no significant overall monthly geometric mean $PM_{2.5}$ concentration trend was found ($p = 0.303$).

Consistent with previous data analysis of particulate matter observations at BGFM in 2010–2011 (Bytnerowicz et al., 2016; Landis et al., 2017) and 2016 (Landis et al., 2018; Wentworth et al., 2018), and comprehensive AOSR epiphytic lichen biomonitoring source apportionment studies in 2008 (Landis et al., 2012) and 2014 (Landis et al., 2019), the impact of wildland fire smoke emissions was again observed during this study period. Many past high concentration $PM_{2.5}$ concentration episodes in the AOSR have been anecdotally associated with wildland

Table 1
Summary of 24-hour integrated Bertha-Ganter Fort McKay Ambient Measurements on 1-in-3-day NAPS filter samping schedule (October 20, 2014 - October 30, 2015).

Analyte	n	Units	Mean	Std Dev	Min	Q1	Median	Q3	Max
$PM_{2.5}$ Mass (Dichot)	110	μg m^{-3}	8.6	11.8	0.8	3.5	5.5	8.9	87.3
$PM_{10-2.5}$ Mass (Dichot)	109	μg m^{-3}	8.5	9.5	0.2	1.4	3.9	12.6	39.1
$PM_{2.5}$ Mass (SHARP)§	109	μg m^{-3}	8.1	11.5	0.5	3.4	5.0	8.7	86.1
$PM_{2.5}$ Black Carbon§	109	μg m^{-3}	0.7	0.6	0.0	0.3	0.5	0.9	3.4
$PM_{2.5}$ UV Carbon§	109	μg m^{-3}	0.7	0.7	0.0	0.3	0.5	0.8	5.1
Sulfur Dioxide§	109	ppb	1.2	1.3	0.0	0.3	0.7	1.4	5.5
Total Reduced Sulfur§	109	ppb	0.6	0.2	0.3	0.4	0.5	0.7	1.6
Nitrogen Oxide§	108	ppb	3.2	5.1	0.0	0.4	1.3	3.3	29.1
Nitrogen Dioxide§	108	ppb	7.7	6.3	0.2	3.1	5.9	10.3	28.2
Oxides of Nitrogen§	108	ppb	10.9	10.7	0.3	3.9	7.5	12.8	49.9
Total Hydrocarbons§	108	ppm	1.9	0.1	1.8	1.9	1.9	2.0	2.6
Non–Methane Hydrocarbons§	108	ppm	0.0	0.0	0.0	0.0	0.0	0.0	0.2
Methane§	108	ppm	1.9	0.1	1.8	1.9	1.9	2.0	2.4
Ozone§	109	ppb	23.1	10.5	3.8	14.8	22.5	30.7	49.6
Ammonia§	108	ppb	0.1	1.2	0.0	0.0	0.0	0.0	12.4

NOTE: Shaded dichotomous sampler results are filter based and were subsequently analyzed by DRC-ICPMS.
§Daily integrated continuous measurements.

fire smoke as large fire events resulted in visible smoke and a characteristic odor (e.g., 2011, 2016), however it is difficult to flag the impacts of smaller or more distant wildfire event impacts solely based on routine ambient measurements. The Aethalometer mean (0.92) and median (0.95) hourly compensated UVPM/BC ratio for the entire study period indicates that on average, carbon aerosol was dominated by heavy-duty vehicle emission BC. The hourly BC, UVPM, and UVPM/BC ratio were stratified as a function of measured $PM_{2.5}$ concentration (Appendix Fig. D.4), and a clear relationship between increasing UVPM/BC ratio and $PM_{2.5}$ concentration over 10 μg m^{-3} was observed. When the hourly $PM_{2.5}$ concentrations over 30 μg m^{-3} ($n = 268$) were evaluated, the mean (1.54) and median (1.51) values for the UVPM/BC ratio significantly increased, suggesting that organic carbon species from biomass combustion was the dominant source of $PM_{2.5}$ during these periods.

The majority of elevated hourly $PM_{2.5}$ concentrations observed during the study period occurred between June 24 and July 13, 2015, with the highest concentration of 472 μg m^{-3} occurring on July 3, 2015 (Appendix Fig. D.5). The concurrent Aethalometer BC and UVPM values are plotted with the $PM_{2.5}$ concentrations showing that in all cases of elevated $PM_{2.5}$, the UVPM is significantly higher than BC suggesting organic carbon from biomass combustion is the major contributing source. Previous PM source apportionment analysis at BGFM (Landis et al., 2017) and an analysis of emissions from the 2016 Horse River Wildfire (Landis et al., 2018) found that NH_3 and TRS were also good tracer species for biomass combustion in the AOSR. For the most part the BGFM NH_3 measurements were below MDL (Table 1), and quantifiable concentrations were only observed over the 99th percentile of the data distribution. All non-zero NH_3 values occurred during the known wildland fire events and were concurrent with elevated UVPM/BC ratio (Appendix Fig. D.6) confirming that NH_3 is an indicator of wildland fire smoke as suggested by Landis et al. (2018).

Delta-C (UVPM - BC) is another metric used to evaluate the impact of biomass combustion on observed $PM_{2.5}$ concentrations based on the organic components of smoke being preferential absorbers of 370 nm light (Allen et al., 2004; Wang et al., 2010; Wang et al., 2011a, 2011b). When all hourly $PM_{2.5}$ concentrations over 40 μg m^{-3} (half of the AAAQG concentration) were plotted versus Delta-C, TRS, and NH_3 (Appendix Fig. D.7) significant relationships were observed for all three tracers of biomass combustion explaining ~77%, 60%, and 58% of the total variability in $PM_{2.5}$ concentration, respectively. These relationships again highlight that wildland fire smoke is the dominant source of elevated $PM_{2.5}$ concentrations observed at BGFM. Visual inspection of Appendix Fig. D.7 revealed what appears to be two separate linear clusters of Delta-C versus $PM_{2.5}$ data. The data from the two main wildland fire events (July 3–4, 2015 and July 11–12, 2015) were isolated, plotted in Appendix Fig. D.8 and Appendix Fig. D.9, and evaluated separately. The wildland fire smoke event impacting the BGFM site between July 3–4 had a Delta-C to $PM_{2.5}$ linear regression slope of 61.16 and a coefficient of determination of 0.966 suggesting that ~97% of the $PM_{2.5}$ measured at the site over that two-day period could be explained by biomass combustion smoke. The wildland fire smoke event impacting the BGFM site between July 11–12 had a Delta-C to $PM_{2.5}$ linear regression slope of 21.19 and ~87% of the $PM_{2.5}$ measured at the site over that two-day period could be explained by biomass combustion smoke. These very different UVPM/BC ratios versus measured $PM_{2.5}$ concentration suggest that different fuels and/or combustion conditions can impact the mass emission and physiochemical properties of emitted particulate matter only days apart consistent with what has been reported by Harrison et al. (2013).

3.2. PAH and PAC monitoring results

3.2.1. Insights from TSP/PUF/XAD data

The TSP-PUF/XAD data provided information that informed analysis of the PM_{10} and $PM_{2.5}$ data. One goal of performing the TSP-PUF/XAD sampling and analysis was to assess the extent of partitioning of PAC analytes between the particulate and vapor phases under the conditions of high-volume sampling, by performing separate extractions and analyses of the TSP filter and PUF/XAD sorbent. This approach has been previously reported by Stracquadanio and Trombini (2006a, 2006b). Partitioning behavior is illustrated in Appendix Fig. D.10, which shows the fraction of each analyte retained on the TSP filter averaged for winter ($n = 8$) and summer ($n = 9$) sampling events; summer for this study was designated as May 1–October 31. Analytes with molecular weights <200 were found to partition entirely or almost entirely into the vapor phase; analytes with molecular weight >240 were fully retained on the TSP filter, and masses in between varied significantly in their partitioning behavior based primarily on ambient temperature. Similar observations have been made in a study of PAHs collected on archived $PM_{2.5}$ filters (Pleil et al., 2004).

It is important to interpret the sampling data for the PM_{10} and $PM_{2.5}$ filters in the context of the TSP-PUF/XAD particulate and vapor phase partitioning data. In particular, data for compounds with molecular weight <200 were not usable due to low retention on the filter; that includes the PAHs through anthracene (MW = 178), as well as the C1-PAHs through phenanthrene (MW = 178) and dibenzothiophene (MW = 184). Analytes that are only partially partitioned to the particulate phase were likely to give highly variable relative recoveries from the filter; these include the C1-dibenzothiophenes, and pyrene and fluoranthene and their C1 analogs. These findings informed our decision to limit species used in PMF modeling to those largely partitioned into the particulate phase.

Summary statistics for PUF/XAD and TSP samples are shown in Appendix Table C.4 for PAHs and Appendix Table C.5 for PACs. Summing the TSP and PUF/XAD data for each sampling event yields a complete profile of ambient PAHs (Appendix Fig. D.11) and PACs (Appendix Fig. D.12) across vapor and particulate phases. Comparison of the averaged winter and summer profiles shows that, apart from greater relative abundance of the more volatile PAHs and PACs in summer (except for the naphthene and the C1- and C2-naphthalenes), the profiles are similar. The principal difference, which is evident in Appendix Fig. D.10, is that many of the 4–6 ring PAHs were found only in the winter time. Thus, although the modified pyrogenic indices of 0.007 and 0.019 for summer and winter, respectively, are consistent with a primarily petrogenic source for ambient PAHs and PACs, elevated pyrogenic PAHs and retene in winter time suggest other sources were contributing in winter. This information was helpful for interpreting results of PMF modeling of PM data.

3.2.2. Size segregated PM sampling results

Ambient $PM_{2.5}$ sum of all PAHs (ΣPAHs) concentrations varied widely over the study period, ranging from 0.071 to 11.5 ng m^{-3} with a median value of 0.405 ng m^{-3}. Ambient $PM_{10-2.5}$ ΣPAH concentrations (calculated by subtracting $PM_{2.5}$ from PM_{10} for each sample pair) were generally lower, ranging from <MDL to 5.19 ng m^{-3} with a median value of 0.046 ng m^{-3}. ΣPAC concentrations were generally higher in both PM size fractions, but were not as strongly loaded into the $PM_{2.5}$ fraction as was observed for PAHs. Summary statistics for PAHs and PACs are presented in Table 2 for $PM_{2.5}$ and Table 3 for $PM_{10-2.5}$.

The PM_{10} (1-in-3) and the TSP (1-in-24) samples provided different size data sets and were generated using different sampling techniques and according to different schedules. However, for 14 of the 17 TSP/PUF/XAD sampling dates, coincident valid PM_{10} samples were collected, and for a small number of analytes, sufficient measurements above the MDL were available for evaluation. Appendix Fig. D.13 depicts the comparison for five analyte groups. The overall data reflect an approximate 1:1 correspondence between the two sample types. None of the analytes for the TSP samples was significantly higher than the PM_{10} samples. Although sample numbers are small, this finding suggests that coarse particles >10 μm are not responsible for transport of a significant proportion of PAHs to the BGFM monitoring site.

Table 2
Statistical summary of PAH and PAC concentrations in Ambient $PM_{2.5}$ (ng m^{-3}) above method detection limit.

Analyte	n	Mean	Std Dev	Min	Q1	Median	Q3	Max
Naphthalene	1	0.0822		0.0822	0.0822	0.0822	0.0822	0.0822
Acenaphthylene	76	0.0050	0.0103	0.0007	0.0022	0.0031	0.0047	0.0904
Acenaphthene	0							
Fluorene	111	0.0253	0.0130	0.0072	0.0159	0.0220	0.0315	0.0764
Phenanthrene	110	0.0813	0.1466	0.0139	0.0354	0.0523	0.0782	1.4582
Anthracene	0							
Fluoranthene	111	0.0691	0.0934	0.0069	0.0205	0.0398	0.0736	0.6562
Pyrene	112	0.1398	0.2853	0.0211	0.0451	0.0670	0.1102	2.6254
Benzo[*c*]phenanthrene	62	0.0199	0.0267	0.0017	0.0050	0.0102	0.0224	0.1454
Benz[*a*]anthracene	112	0.0432	0.0925	0.0008	0.0055	0.0135	0.0375	0.6230
Chrysene	112	0.0961	0.1849	0.0029	0.0184	0.0397	0.0875	1.4069
Benzo[*bj*]fluoranthene	104	0.1336	0.1771	0.0028	0.0418	0.0855	0.1459	1.1339
Benzo[*k*]fluoranthene	103	0.0315	0.0656	0.0005	0.0057	0.0138	0.0290	0.5373
Benzo[*e*]pyrene	110	0.0448	0.0799	0.0017	0.0093	0.0196	0.0443	0.6637
Benzo[*a*]pyrene	73	0.0746	0.1603	0.0064	0.0150	0.0290	0.0583	1.2008
Indeno[1,2,3-*cd*]pyrene	103	0.0356	0.0666	0.0008	0.0062	0.0170	0.0334	0.4802
Dibenz[*a*,*h*]anthracene	51	0.0163	0.0177	0.0046	0.0070	0.0100	0.0183	0.0979
Benzo[*g*,*h*,*i*]perylene	108	0.0440	0.0781	0.0013	0.0091	0.0195	0.0413	0.5995
ΣPAHs	108	0.8022	1.3402	0.1141	0.2520	0.4037	0.7458	11.5226
C2-Naphthalenes A	110	0.0473	0.0339	0.0067	0.0227	0.0363	0.0626	0.1637
C2-Dibenzothiophenes A	112	0.0417	0.0498	0.0058	0.0198	0.0291	0.0411	0.4447
C2-Dibenzothiophenes B	109	0.0821	0.0929	0.0124	0.0300	0.0562	0.0844	0.5962
C2-Phenanthrenes/anthracenes	108	0.3715	0.3577	0.0814	0.1874	0.2544	0.3784	1.9829
C2-Fluoranthenes/pyrenes	109	0.4602	0.4944	0.0559	0.2167	0.2967	0.4935	3.9575
C2-Chrysenes/isomers A	111	0.1199	0.1505	0.0158	0.0501	0.0733	0.1238	1.3614
C2-Chrysenes/isomers B	97	0.0172	0.0219	0.0019	0.0071	0.0114	0.0196	0.1978
C2-Benzopyrenes	57	0.0090	0.0113	0.0015	0.0024	0.0047	0.0102	0.0724
1-Methylnaphthalene	27	0.0093	0.0085	0.0049	0.0060	0.0072	0.0090	0.0501
2-Methylnaphthalene	34	0.0063	0.0054	0.0028	0.0039	0.0045	0.0076	0.0326
C1-Fluorenes	1	0.1718		0.1718	0.1718	0.1718	0.1718	0.1718
Dibenzothiophene	38	0.0359	0.0402	0.0127	0.0147	0.0203	0.0312	0.1980
4-Methyldibenzothiophene	112	0.0207	0.0197	0.0021	0.0101	0.0142	0.0233	0.1055
2/3-Methyldibenzothiophene	109	0.0234	0.0239	0.0034	0.0104	0.0156	0.0242	0.1242
1-Methyldibenzothiophene	112	0.0218	0.0106	0.0043	0.0162	0.0197	0.0246	0.0710
C1-Phenanthrenes	112	0.1596	0.1728	0.0328	0.0887	0.1173	0.1537	1.5685
C1-Fluoranthenes	110	0.1820	0.2197	0.0206	0.0742	0.1104	0.1807	1.4601
C1-Chrysenes	112	0.0928	0.0903	0.0109	0.0425	0.0693	0.1066	0.6371
C1-Benzopyrenes	107	0.0883	0.0887	0.0078	0.0360	0.0635	0.1193	0.6281
ΣPACs	108	1.7176	1.5821	0.3429	0.8965	1.2142	1.8076	9.1390
Retene	112	0.3254	0.7712	0.0140	0.0391	0.0696	0.2178	6.7545

Wildfires in Northern Alberta boreal forests emit substantial amounts of organic aerosols and volatile organic compounds (VOCs) including PAHs (Wentworth et al., 2018), and this source contribution can be assessed using specific marker species, such as retene. The TSP/PUF/XAD sample collected on July 11, 2015 was associated with a wildland fire smoke event (Section 3.3), had a strong retene signal (summing both parts of the sample), and was associated with elevated $PM_{2.5}$, BC, NH_3, and TRS concentrations. The retene spike was accompanied by an increase in total PAHs by a factor of 2–3 times the seasonal average (May–October). The retene signal was also observed in the coincident PM_{10} sample but the concentration was not as high, consistent with primarily vapor phase partitioning of retene in warmer weather. Elevated ΣPAH concentrations are generally associated with wildland fire impact periods even in the most volatile fraction, in spite of those analytes being poorly retained on the filters. Similarly, elevated retene concentrations occur in TSP-PUF/XAD samples from the winter months, possibly associated with wood burning for residential heating or land clearing activities (Landis et al., 2017), and are also accompanied by elevated ΣPAH concentrations even though the overall correlation between the two is relatively low ($r^2 = 0.34$). Again, retene is also elevated in the PM_{10} samples from the winter; in this case, PAHs are also substantially elevated with major contributions from the higher molecular weight PAHs.

The sampling component of this study was designed to improve our understanding of how PAHs and PACs partition among vapor, coarse particulate, and fine particulate phases, and how such partitioning varies over the course of a year. We found that the most abundant PAHs and PACs are of lower molecular weight and higher volatility, and partition into the gas phase in a temperature-dependent manner. The lower molecular weight PAHs and PACs include potential markers differentiating woodsmoke, petrogenic, and pyrogenic sources, so that future sampling for source apportionment modeling should include both a filter and PUF/XAD component. The higher molecular weight PAHs and PACs partition largely or exclusively into the particulate phase and are associated with PM_{10} (as opposed to PM > 10 μm). Within the PM_{10} fraction, data suggested a tendency for PAHs and PACs to be associated with $PM_{2.5}$.

3.3. Inorganic element monitoring results

The inclusion and integration of inorganic emission source tracer species into an integrated PAH receptor modeling framework is beneficial in the AOSR as there is substantially more inorganic source profile information available (Landis et al., 2012; Osacky et al., 2013; Wang et al., 2015; Wang et al., 2016). Consistent with a previous BGFM ambient particulate matter study (Landis et al., 2017), the inorganic analytical techniques utilized were capable of detecting most analytes in both fine and coarse size fractions in >90% of the samples. A statistical summary of $PM_{2.5}$ mass and elements analytes are presented in Table 4. The highest mean concentration was found for Si (361 ng m^{-3}), followed by Ca (229 ng m^{-3}), Fe (117 ng m^{-3}), Al (109 ng m^{-3}), K (66 ng m^{-3}), and Na (51 ng m^{-3}). Mean concentrations of five elements (Ba, Cu, Mn, Ti, Zn) were in the range 1–5 ng m^{-3}, while those for the remaining 30 elements were well below 1 ng m^{-3}. Pb (0.34 ng m^{-3}), As (0.15 ng m^{-3}), Se (0.088 ng m^{-3}) and Cd (0.025 ng m^{-3}) were particularly low relative to literature values from PM studies elsewhere

Table 3
Statistical summary of PAH and PAC concentrations in ambient $PM_{10-2.5}$ (ng m^{-3}) above method detection limit.

Analyte	n	Mean	Std Dev	Min	Q1	Median	Q3	Max
Naphthalene	0							
Acenaphthylene	61	0.0018	0.0090	−0.0477	−0.0001	0.0006	0.0022	0.0309
Acenaphthene	0							
Fluorene	105	0.0090	0.0164	−0.0600	0.0020	0.0071	0.0163	0.0678
Phenanthrene	104	0.0389	0.1184	−0.9042	0.0057	0.0222	0.0642	0.4028
Anthracene	0							
Fluoranthene	107	0.0305	0.1854	−0.1666	−0.0048	0.0034	0.0189	1.8354
Pyrene	107	0.0535	0.2136	−1.0605	−0.0003	0.0204	0.0528	1.2596
Benzo[*c*]phenanthrene	56	0.0123	0.0261	−0.0108	0.0011	0.0029	0.0062	0.1132
Benz[*a*]anthracene	107	0.0258	0.0710	−0.1104	0.0000	0.0045	0.0195	0.4026
Chrysene	107	0.0648	0.2130	−0.5793	−0.0029	0.0077	0.0358	1.2061
Benzo[*bj*]fluoranthene	97	0.0173	0.1767	−0.4918	−0.0495	−0.0072	0.0249	0.6729
Benzo[*k*]fluoranthene	96	0.0146	0.0652	−0.2018	−0.0025	0.0013	0.0116	0.3828
Benzo[*e*]pyrene	106	0.0338	0.0915	−0.3031	0.0021	0.0090	0.0270	0.5331
Benzo[*a*]pyrene	66	0.0569	0.1492	−0.4882	0.0036	0.0119	0.0452	0.6236
Indeno[1,2,3-*cd*]pyrene	96	0.0250	0.0944	−0.2536	0.0010	0.0033	0.0148	0.7744
Dibenz[*a*,*h*]anthracene	45	0.0125	0.0182	−0.0362	0.0020	0.0047	0.0171	0.0691
Benzo[*g*,*h*,*i*]perylene	103	0.0216	0.0642	−0.2708	0.0011	0.0057	0.0207	0.3163
ΣPAHs	108	0.3709	1.05480	−2.8490	−0.0154	0.0522	0.3440	5.1871
C2-Naphthalenes A	104	0.0195	0.0408	−0.0478	−0.0019	0.0081	0.0304	0.2202
C2-Dibenzothiophenes A	106	0.0333	0.0645	−0.0194	0.0053	0.0134	0.0304	0.4664
C2-Dibenzothiophenes B	103	0.0995	0.2458	−0.0496	0.0067	0.0305	0.0782	1.9211
C2-Phenanthrenes/anthracenes	99	0.3142	0.8794	−0.2351	0.0138	0.0897	0.2180	6.2778
C2-Fluoranthenes/pyrenes	101	0.3149	0.6057	−0.6443	0.0132	0.0969	0.3984	2.9999
C2-Chrysenes/isomers A	105	0.1643	0.2892	−0.1255	0.0251	0.0574	0.1434	1.5203
C2-Chrysenes/isomers B	91	0.0199	0.0368	−0.0230	−0.0008 8	0.0068	0.0201	0.1873
C2-Benzopyrenes	49	0.0174	0.0237	−0.0005	0.0022	0.0076	0.0222	0.0975
1-Methylnaphthalene	20	0.0184	0.0196	−0.0011	0.0043	0.0094	0.0328	0.0656
2-Methylnaphthalene	24	0.0080	0.0099	−0.0008	0.0013	0.0042	0.0111	0.0332
C1-Fluorenes	0							
Dibenzothiophene	35	0.0466	0.0793	−0.0106	0.0104	0.0230	0.0455	0.4098
4-Methyldibenzothiophene	107	0.0282	0.0662	−0.0180	0.0033	0.0087	0.0258	0.4979
2/3-Methyldibenzothiophene	105	0.0294	0.0706	−0.0190	0.0028	0.0076	0.0250	0.5063
1-Methyldibenzothiophene	107	0.0163	0.0350	−0.0215	0.0033	0.0070	0.0156	0.2640
C1-Phenanthrenes	107	0.1553	0.4216	−0.1143	0.0114	0.0432	0.1176	3.3482
C1-Fluoranthenes	105	0.1533	0.3903	−0.3208	0.0062	0.0450	0.1207	2.3491
C1-Chrysenes	107	0.0985	0.2480	−0.1961	−0.0050	0.0241	0.0696	1.7887
C1-Benzopyrenes	102	0.0501	0.1348	−0.3443	−0.0100	0.0203	0.0559	0.6686
ΣPACs	108	1.4540	3.2223	−1.2209	0.0886	0.4354	1.1890	20.3593
Retene	106	0.1777	0.5511	−0.6063	0.0040	0.0211	0.0838	3.7256

NOTE: Negative concentration values are a result of field blank subtraction of above MDL sample mass determinations.

(Allen et al., 2001; Makkonen et al., 2010; Hsu et al., 2016; Venter et al., 2016). A statistical summary for mass and trace elements in $PM_{10-2.5}$ samples is presented in Table 5. The most abundant trace elements followed a similar order as for $PM_{2.5}$, but at markedly higher concentrations: Si (1017 ng m^{-3}), Ca (624 ng m^{-3}), Al (340 ng m^{-3}) and Fe (332 ng m^{-3}). Similar to $PM_{2.5}$, the majority of elements exhibited mean concentrations <1 ng m^{-3}. Box and whisker plots depicting fine and coarse fraction trace element concentrations and measures of central tendency are depicted in Appendix Fig. D.14. Across elements, and for both size fractions, the range of concentrations spans 5 orders of magnitude (e.g., from several pg m^{-3} to hundreds ng m^{-3}). The range of observed concentrations for each element covers roughly a factor of 20–30, indicating high day-to-day variability.

Appendix Fig. D.15 shows fine to coarse ratios for average concentrations of mass and elements. A ratio of 1 indicates the analyte is evenly distributed between the two size fractions and ratios greater than or <1 indicate predominance in the fine or coarse fraction, respectively. Results show that mass is evenly divided, but that, in general, individual elements tend to favor one size fraction or the other. >80% of the total (fine + coarse) S and Cd, and >66% of Sb, Pb, and Zn are found in the fine fraction. This is indicative of a photochemical source for S (conversion of SO_2 to sulfate) and high temperature sources for Cd, Sb, Pb, and Zn. Most other elements favor the coarse fraction (>66%), including the crustal and rare earth elements Al, Ca, Si, Ce, La, Nb, Pr, Sm, Th, and U.

The proportion of PM in the fine and coarse fractions can be indicative of the relative importance of primary high temperature anthropogenic emissions and secondary photochemically-formed aerosols versus the physical suspension of soils and material stockpiles through wind-blown or mechanical processes. A time series of 24-hour integrated $PM_{2.5}$ and $PM_{10-2.5}$ masses are depicted in Appendix Fig. D.16, demonstrating a wide range of concentrations for each size fraction as well as high day-to-day variability. $PM_{2.5}$ mass is generally <10 μg m^{-3}, except for sporadic episodes in the fall of 2014 and an extended episode from mid-May to mid-July of 2015 during a major wildfire event. By themselves, the wildland fire samples caused an almost 30% increase in annual $PM_{2.5}$ mass. The annual distribution of $PM_{10-2.5}$ mass differs significantly from $PM_{2.5}$. $PM_{10-2.5}$ mass is uniformly low (and lower than $PM_{2.5}$ mass) from October 2014 through February 2015, but much higher (and typically greater than $PM_{2.5}$) from March through August 2015. The annual pattern of $PM_{10-2.5}$ mass may reflect suppression of resuspended dust when the landscape is covered with snow, and much more active emissions during the summer when soil is bare and soil moisture is low.

Daily average $PM_{2.5}$ and $PM_{10-2.5}$ sulfur concentrations are presented in Appendix Fig. D.17. As indicated previously, S occurs predominantly in the fine fraction as sulfate. Interestingly, 9 of the 10 highest $PM_{2.5}$ sulfur concentrations occur in the winter when photochemical activity is low. Reasons for these wintertime spikes are unclear but might indicate gas to particle conversion of SO_2 during extended fog episodes. Twenty-four-hour average concentrations for three relatively abundant elements in $PM_{2.5}$ and $PM_{10-2.5}$ are shown in Appendix Fig. D.18. The month-to-month patterns for these elements are fairly similar, with

Table 4
Statistical summary of trace elements (ng m^{-3}) in ambient $PM_{2.5}$ above method detection limit.

Analyte	n	Mean	Std Dev	Min	Q1	Median	Q3	Max
Aluminum	110	109.181	127.101	10.844	30.540	59.549	134.488	840.131
Antimony	110	0.068	0.126	0.005	0.019	0.032	0.075	1.064
Arsenic	110	0.146	0.172	0.016	0.061	0.116	0.173	1.605
Barium	108	1.522	1.710	0.169	0.599	1.029	1.664	10.466
Beryllium	42	0.013	0.006	0.007	0.009	0.011	0.016	0.035
Bismuth	100	0.012	0.012	0.003	0.006	0.009	0.014	0.084
Cadmium	107	0.029	0.043	0.003	0.007	0.017	0.029	0.303
Calcium	110	229.09	394.75	38.06	63.44	105.01	234.04	3190.12
Cerium	110	0.120	0.159	0.008	0.030	0.054	0.134	1.014
Cesium	110	0.010	0.011	0.001	0.004	0.006	0.013	0.068
Chromium	94	0.493	0.345	0.159	0.279	0.392	0.595	2.505
Cobalt	110	0.047	0.046	0.004	0.018	0.033	0.062	0.295
Copper	87	1.643	1.346	0.416	0.828	1.262	1.878	9.006
Iron	110	117.69	175.69	9.63	28.55	57.01	129.39	1270.94
Lanthanum	110	0.059	0.074	0.002	0.016	0.033	0.068	0.481
Lead	110	0.346	0.301	0.024	0.107	0.266	0.497	1.669
Lithium	107	0.113	0.140	0.010	0.031	0.057	0.140	0.929
Magnesium	110	28.50	32.88	2.45	8.64	19.38	32.98	210.03
Manganese	110	2.445	2.978	0.247	0.784	1.585	2.956	21.028
Molybdenum	110	0.116	0.111	0.013	0.038	0.072	0.166	0.435
Neodymium	110	0.049	0.067	0.003	0.012	0.023	0.058	0.443
Nickel	90	0.421	0.378	0.136	0.216	0.324	0.458	2.919
Niobium	110	0.015	0.018	0.003	0.005	0.009	0.019	0.116
Palladium	46	0.012	0.006	0.006	0.007	0.009	0.015	0.027
Phosphorus	103	11.948	3.157	7.906	9.918	11.330	12.631	26.711
Platinum	14	0.002	0.001	0.001	0.001	0.002	0.002	0.005
Potassium	110	65.57	78.27	2.99	20.95	38.89	73.18	532.11
Praseodymium	110	0.013	0.018	0.001	0.004	0.006	0.015	0.116
Rubidium	110	0.196	0.233	0.011	0.056	0.119	0.229	1.310
Samarium	108	0.010	0.013	0.001	0.003	0.005	0.012	0.087
Selenium	107	0.088	0.057	0.015	0.052	0.072	0.106	0.294
Silicon	107	361.11	422.74	33.91	118.16	231.41	432.40	2828.19
Sodium	110	51.01	72.75	3.21	12.77	23.84	55.56	544.94
Strontium	110	0.524	0.589	0.045	0.189	0.334	0.605	3.545
Sulfur	110	0.344	0.239	0.024	0.157	0.296	0.458	1.231
Tantalum	60	0.002	0.001	0.001	0.001	0.001	0.002	0.009
Thallium	93	0.005	0.003	0.001	0.002	0.004	0.006	0.021
Thorium	102	0.016	0.020	0.001	0.004	0.008	0.019	0.137
Tin	85	0.652	0.906	0.145	0.229	0.316	0.887	7.630
Titanium	110	4.129	4.977	0.393	1.209	2.220	4.848	32.985
Tungsten	91	0.039	0.071	0.007	0.013	0.022	0.046	0.660
Uranium	105	0.005	0.007	0.001	0.002	0.003	0.006	0.039
Vanadium	110	0.641	0.738	0.042	0.150	0.349	0.892	3.730
Zinc	110	4.768	5.196	0.872	1.944	3.257	5.205	34.934

high $PM_{2.5}$ during the fall of 2014 and high $PM_{10-2.5}$ in the late spring and summer of 2015. K also shows major excursions during the wildfire events in May–July 2015 and some spikes in the fall that are not accompanied by elevated Al or Fe. Given that K is a good tracer for biomass burning, the fall spikes might be an indication of local community residential wood combustion for home heating purposes (Landis et al., 2017). Average concentrations for three low concentration elements (Cd, Pb, and Mo) in $PM_{2.5}$ and $PM_{10-2.5}$ are shown in Appendix Fig. D.19. The seasonal patterns for these elements show very distinct characteristics. Cd is found predominantly in $PM_{2.5}$ and shows elevated concentrations during the winter and especially towards the end of the summer 2015 during the wildfire impacts.

3.4. $PM_{2.5}$ source apportionment results

The PMF model was run using 46 species (9 PAHs, 4 PACs, 31 inorganic elements, BC, and $PM_{2.5}$ mass) for 100 $PM_{2.5}$ samples in common with valid PAH/PAC and trace element data. The model was run with the number of factors ranging from 4 to 7, and the optimum solution was determined to be 6 factors based on explained variance, rotational ambiguity, and model fit statistics. Displacement error analysis found no errors with dQ = 0. Of the 100 block bootstrap runs, >98% mapped to their base factors for all factors except Factor 1 identified as Biomass Combustion which was mapped in 81% of the base runs. Seasonal and episodic characteristics of this factor may explain the observed lower correlations with base runs. The mean normalized factor profiles for those analytes found to be significantly different from zero (bootstrap 5th percentile concentrations were >0) were included in Fig. 2, otherwise the PMF profile concentration, mass explained, and DISP values were set to zero. Temporal plots of factor source contribution estimates (SCEs) are presented in Fig. 3.

$PM_{2.5}$ PMF Factor 1 – Biomass Combustion: This factor is predominantly driven by substantial loadings of Zn (39%), Cd (71%), K (40%), and BC (35%) (Fig. 2a). These elements are consistent with previously reported biomass combustion source profiles in the AOSR (Landis et al., 2012; Landis et al., 2017; Phillips-Smith et al., 2017). In the AOSR, Cd in particular has been found to be strongly associated with both boreal wildfire smoke (Landis et al., 2017) emissions and the residual ash (Landis et al., 2012). UVPM exhibited a Pearson correlation of 0.83 ($p < 0.0001$) supporting the identification of this factor as biomass combustion (Jeong et al., 2004; Sandradewi et al., 2008; Wang et al., 2011a). The SCE of this factor captures impacts of a known wildfire event detected at BGFM between June 29th and July 14th of 2015 (Fig. 3a). In addition to the summer wildland fire events, moderate SCE contributions are also present in winter suggesting contributions from local residential wood combustion for home heating and biomass burning from land clearing activities as previously noted by Landis et al. (2017). Due to the sporadic impact of biomass combustion to the site,

Table 5
Statistical summary of trace elements (ng m^{-3}) in ambient $PM_{10-2.5}$ above method detection limit.

Analyte	n	Mean	Std Dev	Min	Q1	Median	Q3	Max
Aluminum	110	340.041	406.841	8.360	68.030	167.680	443.240	1794.830
Antimony	109	0.027	0.023	0.004	0.011	0.020	0.035	0.143
Arsenic	109	0.081	0.082	0.009	0.024	0.047	0.104	0.391
Barium	108	3.279	3.743	0.134	0.705	1.718	4.715	18.538
Beryllium	77	0.019	0.012	0.008	0.011	0.014	0.025	0.062
Bismuth	73	0.014	0.042	0.002	0.003	0.005	0.009	0.277
Cadmium	94	0.004	0.002	0.001	0.003	0.004	0.005	0.010
Calcium	109	623.693	804.185	46.380	104.270	263.990	819.350	3494.180
Cerium	110	0.384	0.469	0.007	0.065	0.180	0.524	2.151
Cesium	110	0.027	0.034	0.001	0.006	0.012	0.037	0.153
Chromium	86	0.821	0.798	0.177	0.326	0.526	1.195	5.203
Cobalt	87	0.133	0.118	0.021	0.042	0.087	0.194	0.515
Copper	96	2.171	8.837	0.133	0.420	0.707	1.320	85.224
Iron	109	331.614	402.703	11.483	56.678	173.963	464.712	1994.457
Lanthanum	109	0.186	0.227	0.004	0.034	0.092	0.258	1.075
Lead	105	0.167	0.195	0.013	0.055	0.097	0.220	1.256
Lithium	106	0.346	0.413	0.017	0.070	0.152	0.433	1.691
Magnesium	110	74.596	89.478	2.580	14.530	38.395	99.770	420.100
Manganese	108	5.875	6.980	0.259	1.019	2.936	7.934	31.999
Molybdenum	98	0.065	0.051	0.014	0.032	0.049	0.085	0.267
Neodymium	110	0.165	0.204	0.003	0.028	0.079	0.221	0.942
Nickel	73	0.987	2.599	0.194	0.321	0.540	0.899	22.491
Niobium	107	0.047	0.054	0.004	0.010	0.022	0.062	0.258
Palladium	26	0.020	0.011	0.011	0.012	0.015	0.023	0.054
Phosphorus	107	14.155	8.417	4.520	8.150	10.440	18.470	39.910
Platinum	26	0.002	0.001	0.001	0.001	0.002	0.002	0.005
Potassium	109	106.675	123.598	1.644	19.258	56.418	147.828	537.755
Praseodymium	110	0.044	0.053	0.001	0.007	0.021	0.061	0.249
Rubidium	109	0.462	0.573	0.013	0.080	0.210	0.593	2.557
Samarium	110	0.031	0.038	0.001	0.006	0.016	0.040	0.176
Selenium	91	0.118	0.125	0.023	0.039	0.069	0.163	0.904
Silicon	110	1017.447	1103.437	54.610	254.300	536.355	1359.180	4737.850
Sodium	110	55.549	61.070	2.170	15.130	34.335	71.620	359.000
Strontium	110	1.464	1.775	0.043	0.270	0.721	1. 921	7.588
Sulfur	110	0.038	0.036	0.002	0.012	0.026	0.057	0.209
Tantalum	100	0.004	0.004	0.001	0.001	0.002	0.005	0.018
Thallium	106	0.004	0.004	0.000	0.001	0.002	0.005	0.021
Thorium	109	0.052	0.063	0.002	0.010	0.025	0.070	0.291
Tin	59	0.548	0.443	0.082	0.147	0.340	0.945	1.667
Titanium	110	13.430	16.431	0.517	2.439	5.928	18.900	76.505
Tungsten	68	0.076	0.060	0.023	0.035	0.057	0.089	0.284
Uranium	110	0.014	0.017	0.000	0.001	0.003	0.019	0.075
Vanadium	110	0.975	1.102	0.046	0.237	0.497	1.245	4.461
Zinc	101	2.087	2.275	0.552	0.984	1.576	2.506	21.585

the contribution of PAH/PAC species to this factor is <2.5% of the total ΣPAH+PAC species concentrations. During the 2016 Horse River Wildfire Wentworth et al. (2018) noted the measured ΣPAH exceeded baseline concentrations by 3–80 times. During this study we did not observe a significant change in ΣPAH concentration during the five wildfire-impacted sampling days, perhaps due to the distance of the station to the fire source location and the relative lower intensity of impact.

$PM_{2.5}$ PMF Factor 2 – Pyrogenic PAH: High molecular weight PAHs such as chrysene, indeno(1,2,3-c,d)pyrene, benzo(g,h,i)perylene, benzofluoranthenes, and benzopyrenes are loaded on this factor (Fig. 2b), but it only explains 4% of the Σmetals load. Moderate to strong correlations of this factor with TRS ($r^2 = 0.55$, $p < 0.0001$), CH_4 ($r^2 = 0.54$, $p < 0.0001$), and NO_x ($r^2 = 0.72$, $p < 0.0001$) may be indicative of contributions from mine heavy hauler vehicle exhaust emissions (Wang et al., 2016). Plausible sources of PAHs in aerosol may be inferred by concentrations of marker compounds and quantitative diagnostic ratios of paired PAH species due to the distributions of homologues strongly associated with formation mechanisms of carbonaceous aerosol with similar characteristics of organic species (Kavouras et al., 2001). Thus, of the molecular markers available from the subset of PAHs included in PMF modeling, benzo(a)anthracene (BAA), benzo(e)pyrene (BeP), and indeno(1,2,3-cd)pyrene (IP) are kinetically favored products from combustion (pyrogenic) processes, while their respective isomers chrysene, benzo(a)pyrene (BaP), and benzo(g,h,i)perylene (BghiP) are the thermodynamically favored products of petrogenic processes. However, specific ratios are strongly source dependent even when categorizing as pyrogenic or petrogenic, such that use of multiple ratios (e.g., double ratio plots) is more reliable for characterizing different source profiles and matching them to sampling data (Stogiannidis and Laane, 2015). Table 6 illustrates that while the ratios calculated from the Factor 2 profile are consistent with some published pyrogenic sources, they also bear a strong resemblance to petroleum coke and oil sands ore sources in the vicinity of Fort McKay. It is notable, however, that this factor has chrysene concentrations that are three times higher than C2-chrysenes, which is unlike what is observed in petroleum coke or mine ore, where C2-chrysenes are five to ten times more abundant than chrysene (Jariyasopit et al., 2018; Yang et al., 2011). Given the disproportionate representation of the pyrogenic PAHs in this factor, it is identified as a general pyrogenic source.

$PM_{2.5}$ PMF Factor 3 – Fugitive Dust: This factor is identified as Fugitive Dust as it includes most of the crustal elements, indicated by high concentrations of Al, Si, Ti, Fe, Mg, and rare earth elements (Fig. 2c; Reff et al., 2007). Ca in this factor may be attributable to local haul roads used by mine fleet vehicles (Landis et al., 2012). Approximately 74% of the Σmetals are found in this factor, but ΣPAH+PAC are negligible (<1.5%). Negligible contributions from this factor are observed during the winter when the ground surface is snow covered (Fig. 3c), as

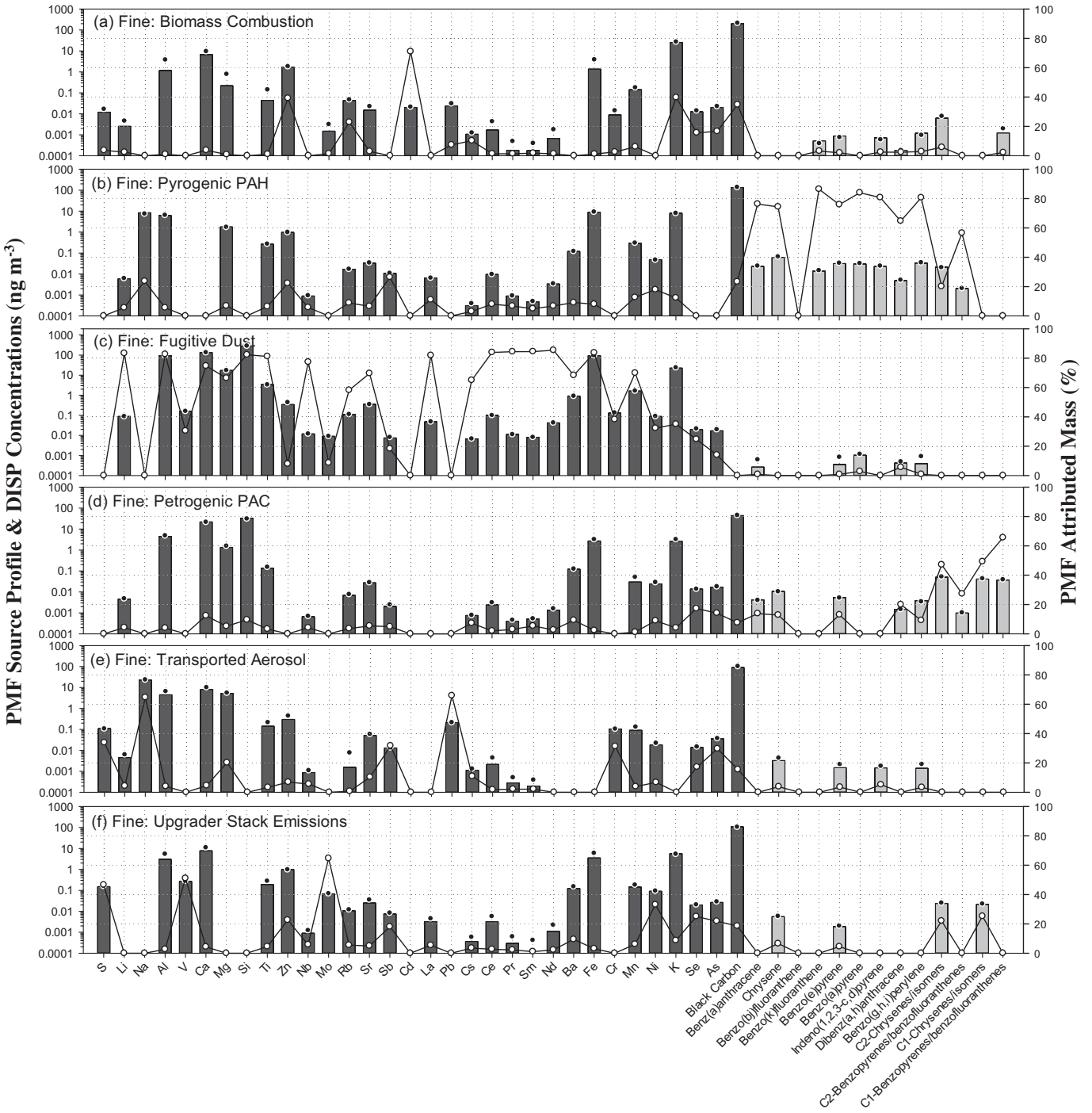

Fig. 2. $PM_{2.5}$ PMF Source Profiles (bars represent concentrations, black circles represent mean DISP values, y-axis on the left; white circles (connected to aid visual interpretation) represent Attributed Mass, y-axis on right).

previously observed by Landis et al. (2017) for fugitive dust impacts at this site.

$PM_{2.5}$ PMF Factor 4 – Petrogenic PAC: This factor is characterized by significant loadings of PACs and BC (Fig. 2d). The C2-chrysene concentration in this factor is about five times the chrysene concentration, consistent with petroleum coke or mine ore; other PACs are also represented in this factor whereas PAHs are much less abundant. Typical oil sand marker elements are missing (e.g., V), but crustal elements are present (e.g., Ba, Sm, Ca, Cs). Furthermore, unlike the Pyrogenic PAH factor, this PAC factor does not exhibit a seasonal trend (Fig. 3d). In the AOSR region, the production of petroleum coke by bitumen upgrading operations is a continuous process. The transportation and storage of petroleum coke are subject to wind erosion year-round and the PM generated is composed of carbon rich particles with PACs (Yang et al., 2011; Jariyasopit et al., 2016; Jariyasopit et al., 2017). However, because it was inappropriate to use measurements of lower molecular weight PACs in the PMF analysis, which would help distinguish petroleum coke from mine ore, it is difficult to specifically assign this factor to either one.

$PM_{2.5}$ PMF Factor 5 – Transported Aerosol: Though elements typically associated with primary anthropogenic emissions such as Pb, S, and Sb are present in this factor (Fig. 2e), no corroborating characteristics of local primary emissions such as correlations with ancillary criteria air pollutant (e.g., NO_x, SO_2) measurements are observed. Seasonality is displayed by this factor contribution (Fig. 3e), with the largest

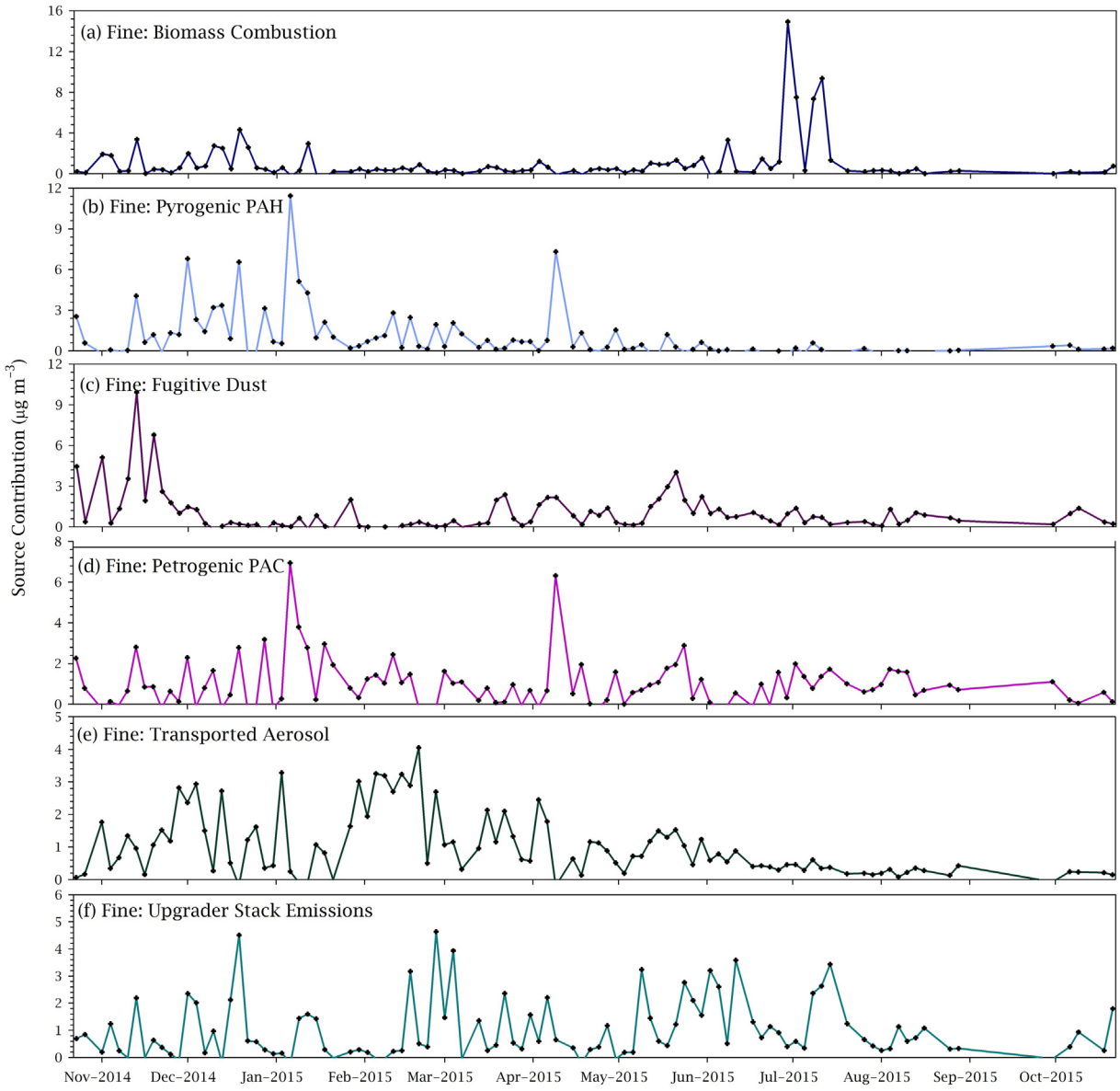

Fig. 3. $PM_{2.5}$ PMF Source Contribution Estimate Time Series.

contributions in winter and spring. The presence of Pb and the seasonality presented is consistent with regional or long-range transport to the AOSR discussed in Graney et al. (2019). Winter road salt is likely mixed with this factor, which is indicated by Na and Mg with Na/Mg ratio >5.

$PM_{2.5}$ PMF Factor 6 – Upgrader Stack Emissions: Tracers of primary fossil fuel combustion aerosol (e.g., S, V, Mo, Ni) along with approximately 10% of the ΣPAH+PACs characterize this factor (Fig. 2f). Relatively strong to moderate Pearson correlations with ambient SO_2 ($r^2 = 0.58$, $p < 0.0001$) and TRS ($r^2 = 0.47$, $p < 0.0001$) concentrations further associates this factor with a local combustion/bitumen upgrader source. The lack of seasonal variation pattern of the mean source contribution further suggests a continuously operating local source (Fig. 3f).

3.5. $PM_{2.5}$ mass apportionment

The PMF model six factor solution explains 82% of the measured $PM_{2.5}$ mass. Although PMF captured a wildfire event in the Biomass Combustion factor, it did not account for a large portion of the $PM_{2.5}$ mass generated by the wildfire event. PMF does not model high transient excursions like impacts from nearfield wildland fire well (Landis et al., 2017) and as a result, 18% of the measured $PM_{2.5}$ mass was unexplained. When apportionment calculations were repeated after

Table 6
Characteristic PAH diagnostic ratios from the literature.

Diagnostic PAH ratios	Petrogenic	Petroleum coke	Raw oil sand	$PM_{2.5}$ PMF factor 2	Pyrogenic	Wood combustion	Petroleum combustion	Diesel soot
BeP/(BaP + BeP)	0.30–0.40	0.41	0.72–1.0	**0.51**	0.60–0.80	0.48		0.42
ICP/(IP + BcP)	<0.2	0.42	0.32–0.41	**0.41**	>0.2		0.2–0.5	0.42
BaA/(BaA + Chr)	<0.2	0.4	0–0.25	**0.27**	>0.35			0.49

References: Yunker et al., 2002; Brandli et al., 2008; Katsoyiannis et al., 2011; Jariyasopit et al., 2018; Wang et al., 1999; Yang et al., 2011

excluding samples collected between June 29 – July 11, 2015 ($n = 5$), the unaccounted mass was reduced to just 5% of the measured mean $PM_{2.5}$ mass. In the absence of wildfire impact period, the predominant sources of $PM_{2.5}$ mass at the BGFM site were (i) Fugitive Dust, with a mean concentration of 1.86 μg m^{-3} accounting for 28% of the $PM_{2.5}$ mass, (ii) Biomass Combustion (1.49 μg m^{-3} and 22%), (iii) Upgrader Stack Emissions (1.44 μg m^{-3} and 21%), (iv) Petrogenic PAH (1.20 μg m^{-3} and 18%), and (v) Transported Aerosol (0.43 μg m^{-3} and 6%). The Pyrogenic PAH source does not account for significant $PM_{2.5}$ mass. If we assume the unexplained mass on wildfire impacted days (n = 5) was contributed by the fire, then the PMF model explains 95% of the measured $PM_{2.5}$ mass and the estimated Biomass Burning source contribution increases to 3.57 μg m^{-3} (a 40% annualized $PM_{2.5}$ mass contribution).

The SWIM model analysis indicates that the highest probability source locations of $PM_{2.5}$ concentrations contributing to measurements at the BGFM monitoring site are the oil sands production facilities located to the north and south of Fort McKay (Fig. 4a). To the northwest of the monitoring site, operations at the Canadian Natural Resources Limited Horizon Mine appear to have a greater contribution than the Syncrude Aurora North Mine; however, the overwhelming majority of the $PM_{2.5}$ mass is contributed from the Suncor and Syncrude operations

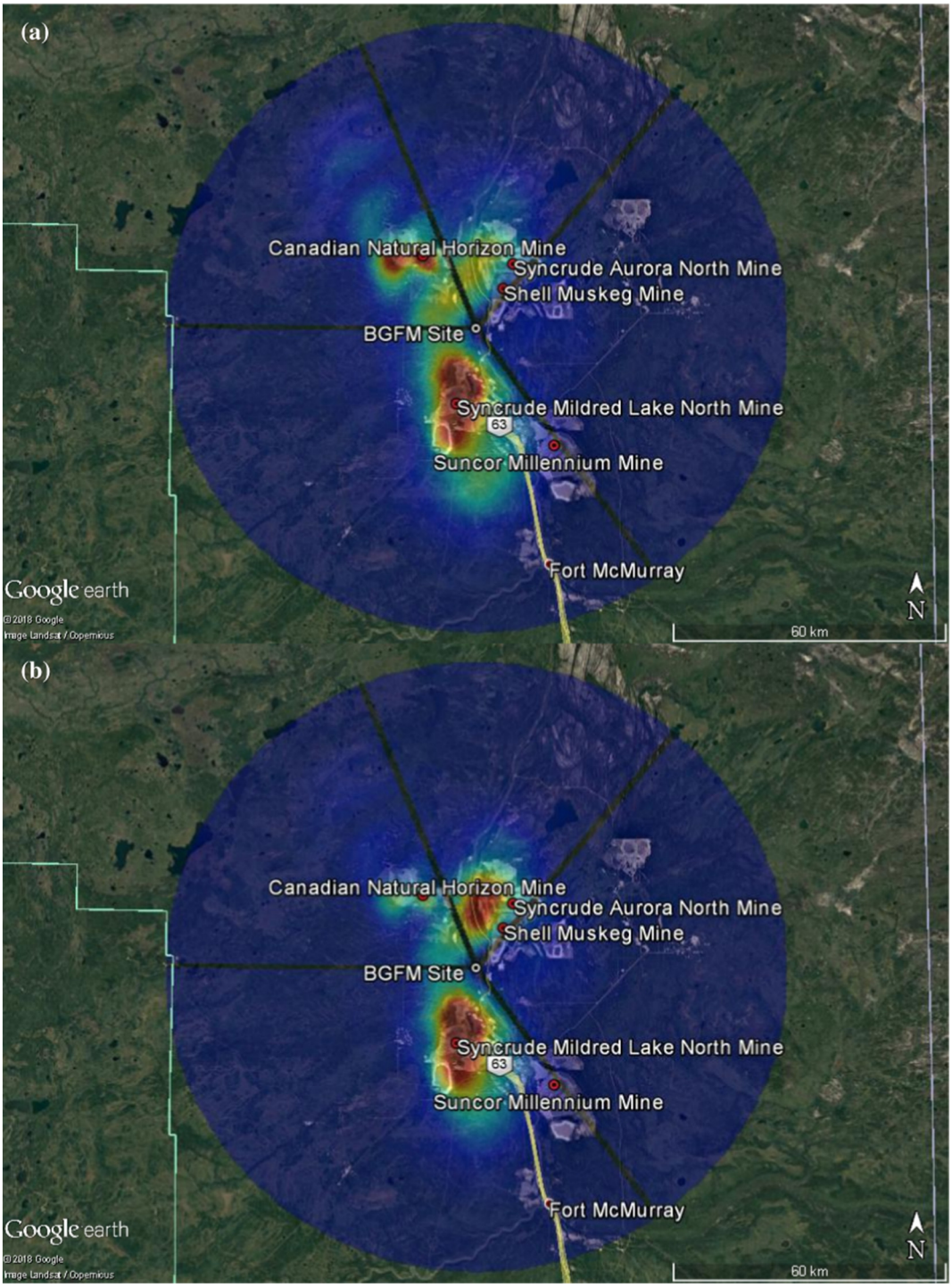

Fig. 4. SWIM Model Spatial Source Probability for (a)$PM_{2.5}$, and (b) BC.

to the south. Unlike $PM_{2.5}$, BC shows a stronger signal north of Fort McKay over the Aurora North Mine and a weaker signal from the Canadian Natural Resources Limited Horizon Mine to the northwest (Fig. 4b).

As discussed in Section 3.3, Delta-C is an indicator for biomass combustion from residential wood combustion (RWC) and wildland fire emissions. Given the size and intensity of the wildland fire signal between June and July 2015, the SWIM model was run separately for Delta-C during the smoke impact period (Fig. 5a) and the rest of the study period (Fig. 5b). The Delta-C signal from the northwest was likely driven by the wildland fires during June and July, with the strongest source contribution area of Delta-C in non-smoke impacted periods coming primarily from the Syncrude Mildred Lake facility area south of Fort McKay. Additionally, the source location of NH_3 contribution to BGFM was evaluated. As previously discussed, the NH_3 instrument reported predominantly non-detects during the study period, except for when the site was impacted by wildland fire smoke emissions. The SWIM model plot for NH_3 (Appendix Fig. D.20) shows a similar probability field as Delta-C during the fire impact period with the exception of a more defined secondary lobe northeast of the Horizon Mine. This may be largely due to the fact that the wildland fire smoke impacts were observed for a relatively short period of time, and that the wildfire was the sole source of elevated ambient NH_3 observed at BGFM.

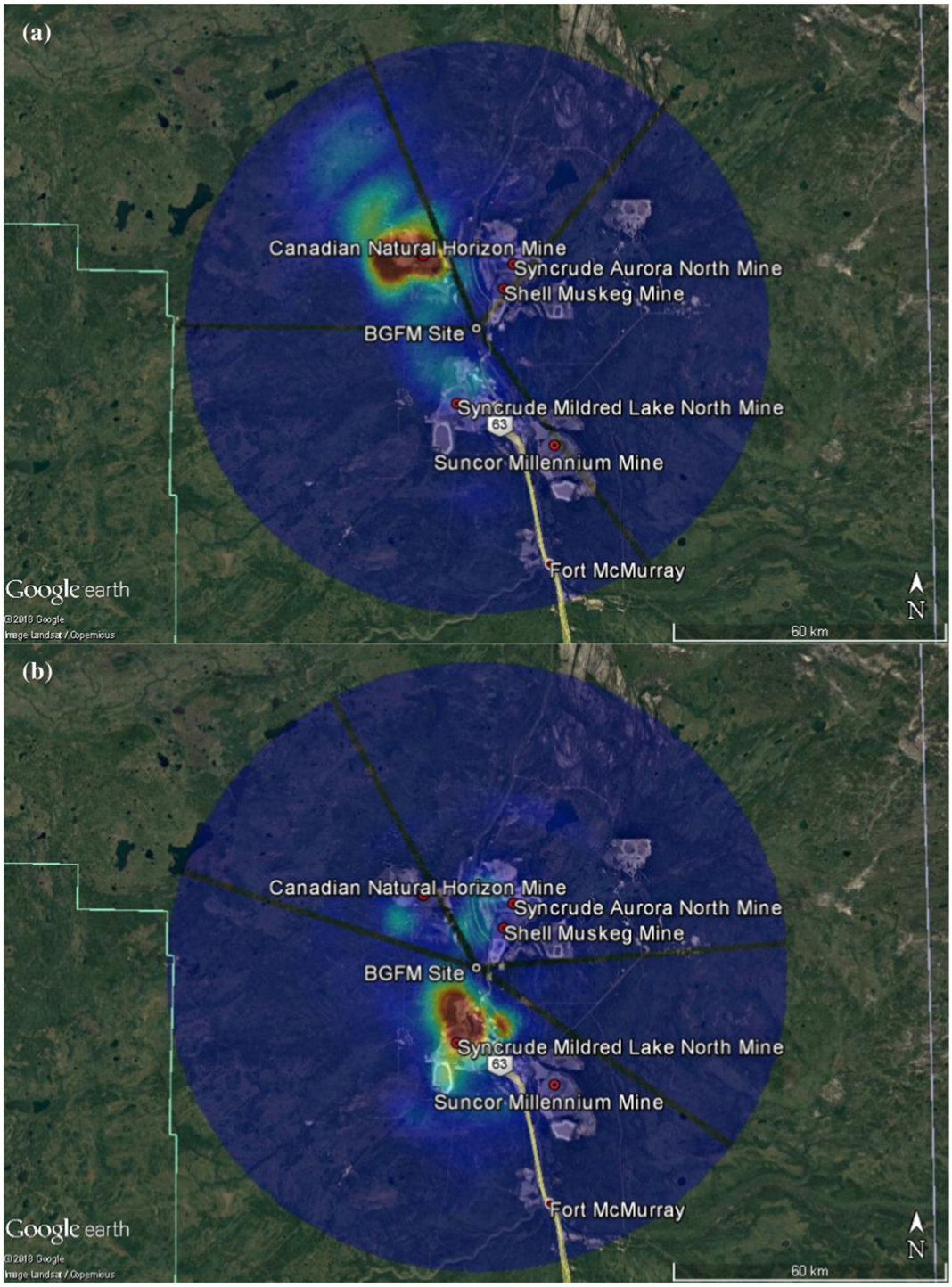

Fig. 5. SWIM Model Spatial Source Probability for Delta-C (a) June–July 2015 and (b) Remainder of Study Period.

Measured concentrations of $PM_{2.5}$ ΣPAH and a multiple linear regression (MLR) analyses were performed with ΣPAH as dependent variable and the individual $PM_{2.5}$ PMF factor contribution estimates as independent variables. The analysis concluded that only the pyrogenic PAH source factor significantly contributed (78%) to the measured $PM_{2.5}$ ΣPAH, while not significantly contributing to the $PM_{2.5}$ mass.

3.6. $PM_{10-2.5}$ PMF source apportionment results

The PMF model was run for $PM_{10-2.5}$ after (i) setting Mo, Cr, Ni, Se and all PAH/PACs to Weak (signal-to-noise in the 1–3 range), (ii) Cd and C2-Chrysene were excluded (signal-to-noise <1), and extra modeling uncertainty of 5% was applied. A 5-Factor solution utilizing 44 species was found to be optimal in terms of explained variance, rotational ambiguity (no factor swaps until dQ = 24), and model fit statistics. Of the 100 bootstrap runs, factors 1 and 3 identified as Organic Aerosol PAH/PAC and Mobile Sources, respectively, mapped to their base factors in 76 and 82 of the runs. Seasonal and episodic characteristics of these factors may explain the observed lower correlations with base runs. All other factors mapped to their base runs in >95 runs. The mean normalized factor profiles for those analytes found to be significantly different from zero were included in Fig. 6 if the bootstrap 5th percentile concentrations were > 0, otherwise the PMF profile concentration, mass explained, and DISP values were set to zero. Temporal plots of factor SCEs are presented in Fig. 7.

$PM_{10-2.5}$ PMF Factor 1 - Organic Aerosol: This factor was loaded with 90% of the total ΣPAH+ΣPAC, while the sum of all metals found in this factor is <1% (Fig. 6a). As was observed with the $PM_{2.5}$ Pyrogenic PAH factor, this factor also displayed SCE seasonality with high contributions in the winter (Oct 25th 2014 – Apr 30th 2015; $n = 60$) and negligible contributions in the summer (May 1st 2015 – Nov 1st 2015; $n = 40$; Fig. 7a). IP/(IP + BghiP) = 0.32; BeP/(BeP + BaP) = 0.55; and BaA/(BaA + chrysene) of 0.35 are ambiguous in the context of the local source profiles in Table 6.

$PM_{10-2.5}$ PMF Factor 2 - Mixed Source Fugitive Dust: Soil elements Al, Ca, Mg, Si, Ti, and Sr along with rare-earth elements are loaded in this factor (Fig. 6b). These elements are the major constituents of airborne soil and road dust, and usually make an important contribution to coarse aerosol (Reff et al., 2007). This factor resembles the source identified as "Mixed Source Fugitive Dust" in the Landis et al. (2017)

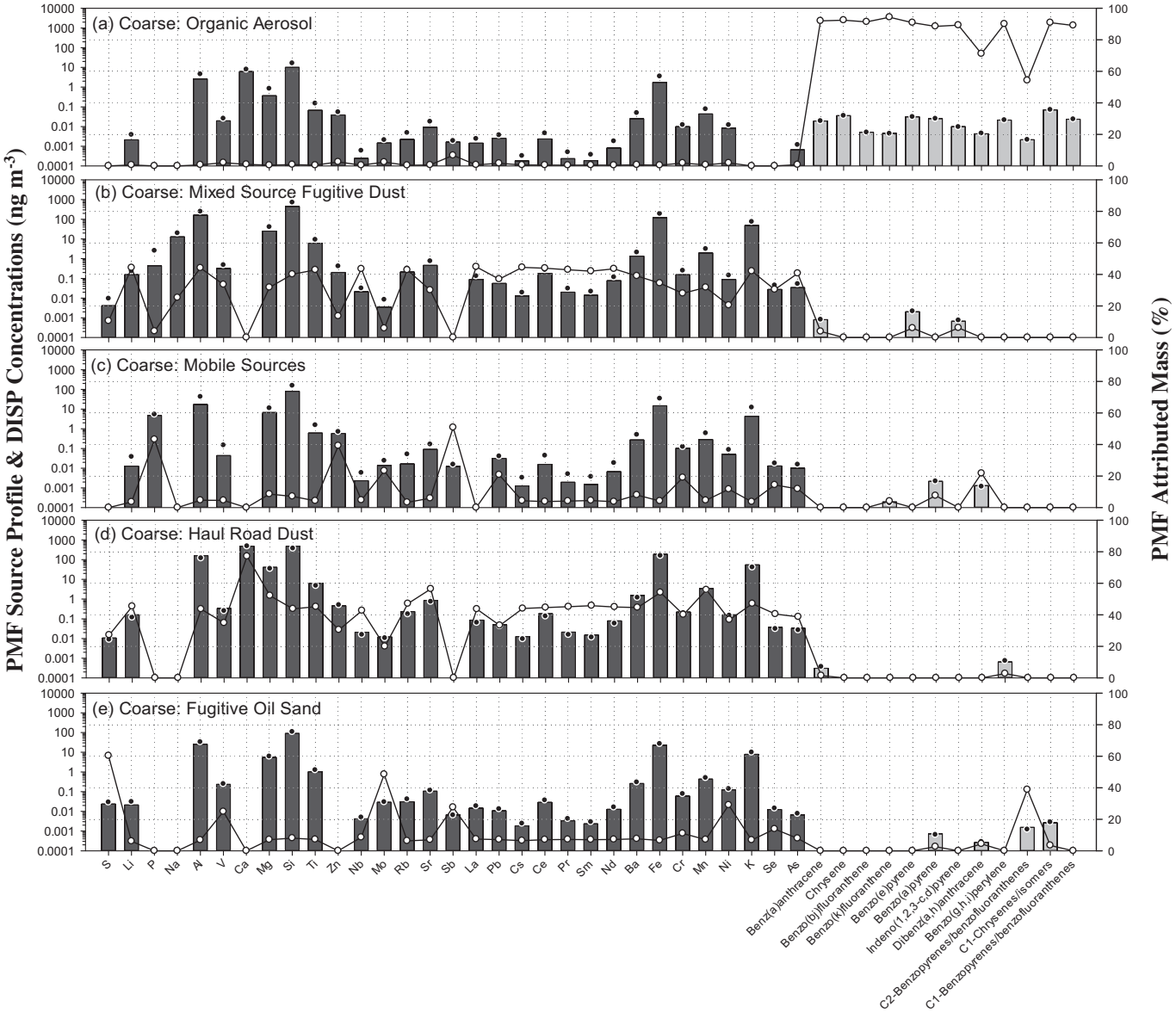

Fig. 6. $PM_{10-2.5}$ PMF Source Profiles (bars represent concentrations, black circles represent mean DISP values, y-axis on the left; white circles (connected to aid visual interpretation) represent % Attributed Mass, y-axis on right).

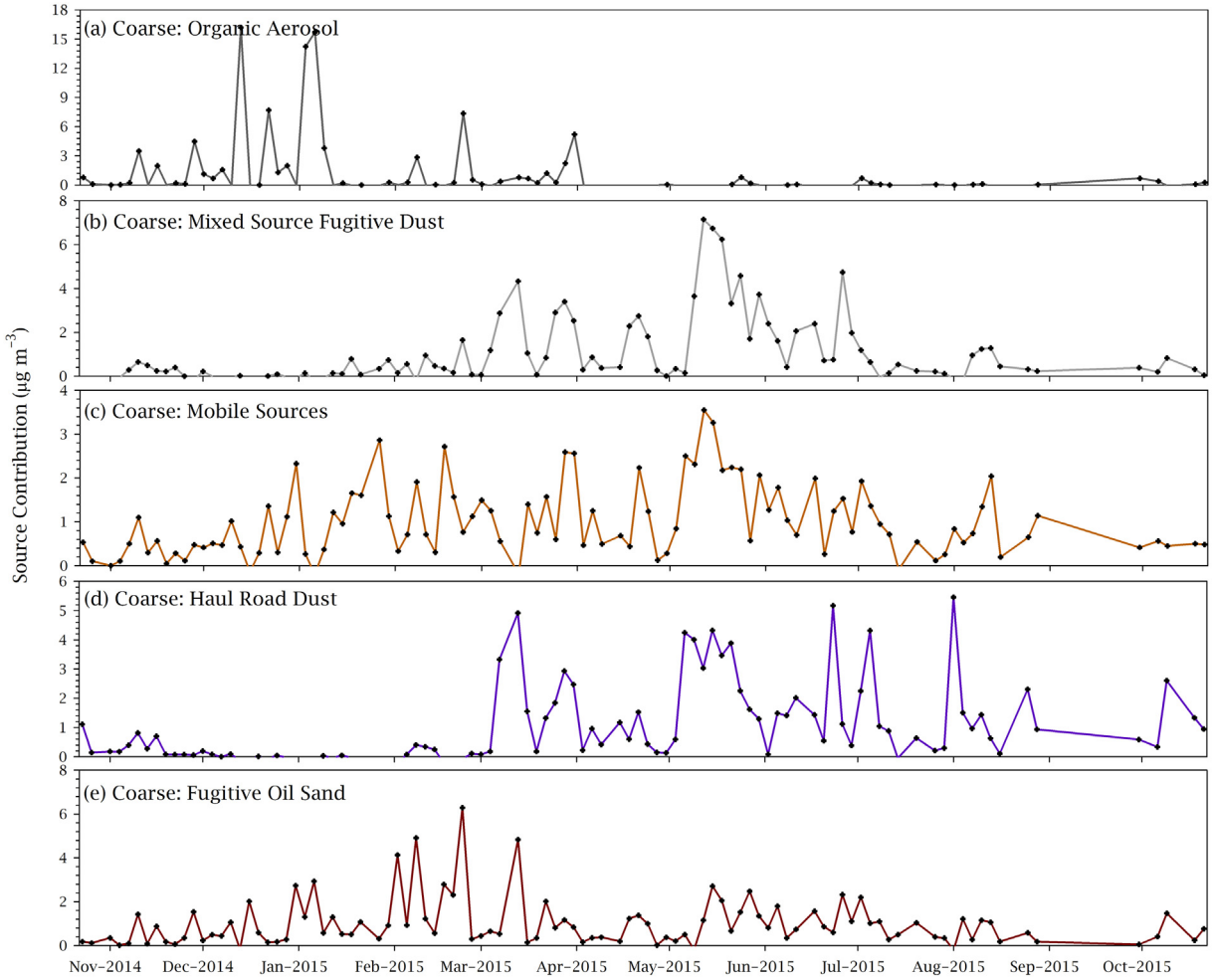

Fig. 7. $PM_{10-2.5}$ PMF Source Contribution Estimate Time Series.

2010–2011 BGFM site inorganic $PM_{10-2.5}$ source apportionment study. The seasonal trends showing low contributions in the winter when the ground is frozen and snow covered is consistent with the other identified fugitive dust sources (Fig. 7b).

$PM_{10-2.5}$ PMF Factor 3 - Mobile Sources: This factor (Fig. 6c) has significant loadings for P (43%), Zn (39%), Sb (50%), Ba (10%) and Pb (20%). These elements have been associated with exhaust emissions and coarse fraction brake and tire wear particulate emissions in other studies (Garg et al., 2000; Wik and Dave, 2009; Gietl et al., 2010; Kreider et al., 2010; Grigoratos and Martini, 2015). Ba and Zn are also found in diesel fuel in the AOSR (Landis et al., 2012). Tire wear is likely to result in predominantly carbonaceous particles, although small quantities of metals, in particular Zn that is used as a vulcanization activator, may be present (Wik and Dave, 2009). Furusjo et al. (2007) suggested that vehicular emissions are associated with high concentrations of Cu, Zn, and Sb. Therefore, this factor was identified as a Mobile Sources factor. The SCE temporal trend (Fig. 7c) shows contributions throughout the year. Since oil sand mining and processing is continuous, emissions from local light-duty road traffic and diesel heavy-duty hauler mine fleets were also expected to be continuous as these SCE results suggest.

$PM_{10-2.5}$ PMF Factor 4 – Haul Road Dust: This factor is driven by 77% loading in Ca (Fig. 6d), but other elemental concentration contributions (e.g., Ti, Rb, La, Cs) and the temporal contribution pattern (Fig. 7d) resemble the Factor 2 Mixed Source Fugitive Dust factor. The inorganic elemental profile abundance in this factor indicates the presence of limestone and resembles the haul road source profiles. The mined limestone in the AOSR is used along with low-grade oil sand to construct temporary mine roads for heavy-duty hauler traffic. Therefore, this factor is regarded as resuspended haul road dust. Earlier studies at BGFM (Landis et al., 2017; Phillips-Smith et al., 2017) have reported similar observations.

$PM_{10-2.5}$ PMF Factor 5 – Fugitive Oil Sand: This factor (Fig. 6e) contains elements associated with bitumen: V (25%), Ni (29%), S (60%), Se (47%), and Mo (49%). Crustal elements such as Al, Si, Fe, Ti, La, and Ce are also present but at relatively low (5–10%) loadings. Alkyl derivatives of benzofluoranthene and chrysene are also found in this factor. SCE from this factor are seen throughout the year with large temporal variability indicating that it is likely representative of mechanically generated fugitive dust from oil sand mining and hauling operations (Fig. 7e).

3.7. $PM_{10-2.5}$ mass apportionment

The PMF model five factor solution explains 98% (8.88 μg m^{-3}) of the mean measured $PM_{10-2.5}$ mass (9.08 μg m^{-3}). The predominant sources of $PM_{10-2.5}$ mass at the BGFM site were (i) Haul Road Dust accounting for 4.82 μg m^{-3} (53% of the measured mass), (ii) Mixed Fugitive Dust (2.89 μg m^{-3} and 32%), (iii) Fugitive Oil Sand (0.88 μg m^{-3} and 10%), Mobile Sources (0.23 μg m^{-3} and 2%), and Organic Aerosol (0.06 μg m^{-3} and 1%). Overall PMF-modeled fugitive dust sources accounted for 95% of the measured $PM_{10-2.5}$ mass at the BGFM site. It should be noted that wildfire impacts between June 29 and July 14, 2015 had a negligible impact on ambient $PM_{10-2.5}$ concentration at BGFM unlike the results reported during the 2011 Richardson Backcountry Wildfire (Bytnerowicz et al., 2016; Landis et al., 2018). The 2011 wildfire was much closer to Fort McKay likely resulting in resuspended $PM_{10-2.5}$ ash reaching BGFM that was not observed during the

2015 wildfire. The MLR analysis was performed with ΣPAH as the dependent variable and the individual PMF $PM_{10-2.5}$ factor contribution estimates as the independent variables. The analysis concluded that only the Organic Aerosol factor significantly contributed (86%) to the measured ΣPAH.

4. Conclusions

A comprehensive database of ambient filter-based particulate matter PAHs, PACs, trace elements, and BC concentrations was developed from October 2014–October 2015 as part of a source apportionment study conducted in the Fort McKay First Nation and Metis community. The BGFM community monitoring station is located in close proximity to several oil sand production operations and was previously found to be impacted by air emissions from oil sand production operations. During the study period the mean $PM_{2.5}$ concentration was 8.6 ± 11.8 μg m^{-3}, and the mean $PM_{10-2.5}$ concentration was 8.5 ± 9.5 μg m^{-3}. Historical data analysis suggests the frequency of wildland fire impacted exceptional $PM_{2.5}$ mass events has been increasing over the last decade. The multi-wavelength Aethalometer deployed during this study shows promise for distinguishing the impact of biomass smoke from petrogenic BC sources. Wind regression analysis found that (i) the oil sand production facilities surrounding BGFM are significant sources of $PM_{2.5}$ and BC, and (ii) wildfire and/or biomass burning associated with land clearing activities to the northwest of the site were significant sources of the highest $PM_{2.5}$ (>10 μg m^{-3}) and BC events measured at the site.

The variable gas/particle partitioning behavior of PAHs and PACs during this study limited our inclusion of quartz filter-based analytes to 13 species with molecular weights above about 240 AMU into the PMF receptor modeling analysis. The $PM_{2.5}$ PMF model six factor solution explained 95% of the measured mass and 78% of the measured ΣPAH after adjustments to account for the unexplained mass for samples ($n = 5$) affected by a summer wildfire event. Five sources were found to contribute significantly to $PM_{2.5}$ mass including (i) Biomass Combustion, with a mean concentration of 3.57 μg m^{-3} accounting for 40%, (ii) Fugitive Dust, (1.86 μg m^{-3} and 28%), (iii) Stack Emissions (1.44 μg m^{-3} and 21%), (iv) Petrogenic PAH (1.20 μg m^{-3} and 18%), and (v) Transported Aerosol (0.43 μg m^{-3} and 6%). However, the analysis concluded that only the Pyrogenic PAH source factor significantly contributed (78%) to the measured ΣPAH, while not significantly contributing to the $PM_{2.5}$ mass. A five-factor PMF model dominated by fugitive dust sources explained 98% of $PM_{10-2.5}$ mass and 86% of the ΣPAH. The predominant sources of $PM_{10-2.5}$ mass were (i) Haul Road Dust (4.82 μg m^{-3} and 53% of the measured mass), (ii) Mixed Fugitive Dust (2.89 μg m^{-3} and 32%), (iii) Fugitive Oil Sand (0.88 μg m^{-3} and 10%), (iv) Mobile Sources (0.23 μg m^{-3} and 2%), and (v) Organic Aerosol (0.06 μg m^{-3} and 1%). Only the Organic Aerosol source significantly contributed (86%) to the measured ΣPAH.

This ambient PM filter-based source apportionment approach yielded only one significant source of PAHs for each of $PM_{2.5}$ and $PM_{10-2.5}$ size fractions, which is in stark contrast to a recent lichen biomonitor receptor modeling study that concluded that (i) multiple sources contributed to the ΣPAH atmospheric deposition, and (ii) lower molecular weight PAC species were critical in resolving some oil sand production sources such as fugitive dust from petroleum coke storage piles in the lichen samples (Landis et al., 2019). Improved source resolution for future ambient PM studies will require the inclusion of important lower molecular weight PAH and PAC tracer species that are semi-volatile, requiring the implementation of a modified sampling methodology that includes PUF/XAD sampling media to consistently captures these analytes. The comparison of TSP and PM_{10} analyte concentrations, while encompassing a smaller data set, suggests that there is little contribution of PAHs or PACs with super micron particles >10 μm at the BGFM site as previously reported for other locations in the AOSR (Zhang et al., 2016).

Acknowledgements

This work was funded by the Wood Buffalo Environmental Association (WBEA), Fort McMurray, Alberta, Canada through contract AA108-17. The content and opinions expressed by the authors do not necessarily reflect the views of the WBEA or of the WBEA membership. We thank Gary Cross (WBEA) for managing the ambient sample collection activities in the AOSR; Sanjay Prasad (WBEA) for providing Bertha Ganter Fort McKay monitoring site ancillary ambient measurement data used in our analysis; Zack Eastman, Hayley Drake, and Kendra Thomas (WBEA) for ambient sample support; Brad Edgerton (ARA) for filter weighing, and Mike Fort (ARA) for dichotomous sampler filter extraction and DRC-ICPMS analysis; Keith Briggs (RTI) for filter preparation and extraction; Michelle McCombs and Cynthia Salmons (RTI) for TOF analysis and TOF data QA review, respectively.

Appendix A. Supplementary data

Supplementary data to this article can be found online at https://doi.org/10.1016/j.scitotenv.2019.02.126.

References

Ahad, J.M.E., Jautzy, J.J., Cumming, B.F., Das, B., Laird, K.R., Sanei, H., 2015. Sources of polycyclic aromatic hydrocarbons (PAHs) to northwestern Saskatchewan lakes east of the Athabasca Oil Sands. Org. Geochem. 80, 35–45.

Alberta Energy, June 2017. Energy: Annual Report 2016-2017. Government of Alberta https://open.alberta.ca/dataset/cbd7147b-d304-4e3e-af28-78970c71232c/resource/7f360403-7e80-40c9-8f7a-0a5079d14f55/download/2016-17-Annual-Report-Energy.pdf, Accessed date: 25 July 2017 (ISBN 1703-4582).

Alberta Energy Regultor, ST98, 2017. Alberta's Energy Reserves & Supply/Demand Outlook. Government of Alberta http://www1.aer.ca/st98/data/executive_summary/ST98-2017_Executive_Summary.pdf, Accessed date: 25 July 2017.

Allen, A.G., Nemitz, E., Shi, J.P., Harrison, R.M., Greenwood, J.C., 2001. Size distributions of trace metals in atmospheric aerosol in the United Kingdom. Atmos. Environ. 35, 4581–4591.

Allen, G.A., Babich, P., Poirot, R.L., 2004. Evaluation of a new approach for real-time assessment of woodsmoke PM. Proceedings of the Regional and Global Perspectives on Haze: Causes, Consequences, and Controversies. Air and Waste Management Association Visibility Specialty Conference, Asheville, NC, paper 16.

Bari, M.A., Kindzierski, W.B., Cho, S., 2014. A wintertime investigation of atmospheric deposition of metals and polycyclic aromatic hydrocarbons in the Athabasca Oil Sands Region, Canada. Sci. Total Environ. 485-486, 180–192.

Birks, S.J., Cho, S., Taylor, E., Yi, Y., Gibson, J.J., 2017. Characterizing the PAHs in surface waters and snow in the Athabasca region: implications for identifying hydrological pathways of atmospheric deposition. Sci. Total Environ. 603-604, 570–583.

Boutin, C., Carpenter, D.J., 2017. Assessment of wetland/upland vegetation communities and evaluation of soil-plant contamination by polycyclic aromatic hydrocarbons and trace metals in regions near oil sands mining in Alberta. Sci. Total Environ. 576, 829–839.

Brandli, R.C., Bucheli, T.D., Ammann, S., Desaules, A., Keller, A., Blum, F., Stahel, W.A., 2008. Critical evaluation of PAH source apportionment tools using data from the Swiss soil monitoring network. J. Environ. Monit. 10, 1278–1286.

Bytnerowicz, A., Hsu, Y.M., Percy, K., Legge, A., Fenn, M.E., Schilling, S., Fraczek, W., Alexander, D., 2016. Ground-level air pollution changes during a boreal wildland mega-fire. Sci. Total Environ. 572, 755–769.

Davidson, C., Spink, D., 2018. Alternate approaches for assessing impacts of oil sands development on air quality: a case study using the First Nation Community of Fort McKay. J. Air Waste Manage. Assoc. 68 (4), 308–328. https://doi.org/10.1080/10962247.2017.1377648.

Droppo, I.G., di Cenzo, P., Power, J., Jaskot, C., Chambers, P.A., Alexander, A.C., Kirk, J., Muir, D., 2018. Temporal and spatial trends in riverine suspended sediment and associated polycyclic aromatic compounds (PAC) within the Athabasca oil sands region. Sci. Total Environ. 626, 1382–1393.

Edgerton, E.S., Fort, J.M., Baumann, K., Graney, J.R., Landis, M.S., Berryman, S., Krupa, S., 2012. Method for extraction and multi-element analysis of *Hypogymnia physodes* samples from the Athabasca Oil Sands Region. In: Percy, Kevin (Ed.), Alberta Oil Sands: Energy, Industry and the Environment. Elsevier, Oxford, England, pp. 315–342.

Fernie, K.J., Marteinson, S.C., Chen, D., Eng, A., Harner, T., Smits, J.E.G., Soos, C., 2018. Elevated exposure, uptake and accumulation of polycyclic aromatic hydrocarbons by nestling tree swallows (Tachycineta bicolor) through multiple exposure routes in active mining-related areas of the Athabasca oil sands region. Sci. Total Environ. 626, 1382–1393.

Foster, K.R., Davidson, C., Spink, D., 2019. Monitoring ecological responses to air quality and deposition in the Athabasca Oil Sands Region: the Wood Buffalo Environmental Association's terrestrial environmental effects monitoring program. Sci. Total Environ. (In Review).

Furusjo, E., Sternbeck, J., Cousins, A.P., 2007. PM_{10} source characterization at urban and highway roadside locations. Sci. Total Environ. 387, 206–219.

Galarneau, E., 2008. Source specificity and atmospheric processing of airborne PAHs: implications for source apportionment. Atmos. Environ. 42, 8139–8149.
Garg, B., Cadle, S.H., Mulawa, P.A., Groblicki, P.J., Laroo, C., Parr, G.A., 2000. Brake wear particulate matter emissions. Environ. Sci. Technol. 34, 4463–4469.
Gietl, J.K., Lawrence, R., Thorpe, A.J., Harrison, R.M., 2010. Identification of brake wear particles and derivation of a quantitative tracer for brake dust at a major road. Atmos. Environ. 44, 141–146.
Graney, J.R., Edgerton, E.S., Landis, M.S., 2019. Using Pb isotope ratios of particulate matter and epiphytic lichens from the Athabasca Oil Sands Region in Alberta, Canada to quantify local, regional, and global Pb source contributions. Sci. Total Environ. 654, 1293–1304.
Grigoratos, T., Martini, G., 2015. Brake wear particle emissions: a review. Environ. Sci. Pollut. Res. Int. 22, 2491–2504.
Harner, T., Rauert, C., Muir, D., Schuster, J., Hsu, Y.M., Zhang, L., Marson, G., Watson, J.G., Ahad, J., Cho, S., Jariyasopit, N., Kirk, J., Korosi, J., Landis, M.S., Martin, J., Zhang, Y., Fernie, K., Wentworth, G.R., Wnorowski, A., Dabek, E., Charland, J.P., Pauli, B., Wania, F., Galarneau, E., Cheng, I., Makar, P., Whaley, C., Chow, J.C., Wang, X., 2018. Air synthesis review: polycyclic aromatic compounds in the Oil Sands Region. Environ. Rev. 26 (4), 430–468.
Harrison, R.M., Beddows, D.C.S., Jones, A.M., Calvo, A., Alves, C., Pio, C., 2013. An evaluation of some issues regarding the use of Aethalometers to measure woodsmoke concentrations. Atmos. Environ. 80, 540–548.
Henry, R.C., Norris, G.A., Vedantham, R., Turner, J., 2009. Source region identification using kernel smoothing. Environ. Sci. Technol. 45, 4090–4097.
Hsu, Y.M., Harner, T., Li, H., Fellin, P., 2015. PAH measurements in air in the Athabasca Oil Sands Region. Environ. Sci. Technol. 49, 5584–5592.
Hsu, C., Chiang, H., Lin, S., Chen, M., Lin, Y., Chen, C., 2016. Elemental characterization and source apportionment of PM_{10} and $PM_{2.5}$ in the western coastal area of central Taiwan. Sci. Total Environ. 541, 1139–1150.
Jariyasopit, N., Harner, T., Wu, D., Williams, A., Halappanavar, S., Su, K., 2016. Mapping indicators of toxicity for polycyclic aromatic compounds in the atmosphere of the Athabasca Oil Sands Region. Environ. Sci. Technol. 50, 11282–11291.
Jariyasopit, N., Zhang, Y., Martin, J.W., Harner, T., 2017. Comparison of polycyclic aromatic compounds in air measured by conventional passive and passive dry deposition samplers and contributions from petcoke and oil sands ore. Atmos. Chem. Phys. Discuss. https://doi.org/10.5194/acp-2017-735 (in review, 2017).
Jariyasopit, N., Zhang, Y., Martin, J.W., Harner, T., 2018. Comparison of polycyclic aromatic compounds in air measured by conventional passive air samplers and passive dry deposition samplers and contributions from petcoke and oil sands ore. Atmos. Chem. Phys. 18, 9161–9171.
Jautzy, J., Ahad, J.M., Gobeil, C., Savard, M.M., 2013. Century-long source apportionment of PAHs in Athabasca oil sands region lakes using diagnostic ratios and compound-specific carbon isotope signatures. Environ. Sci. Technol. 47, 6155–6163.
Jautzy, J.J., Ahad, J.M., Hall, R.I., Wiklund, J.A., Wolfe, B.B., Gobeil, C., Savard, M.M., 2015. Source apportionment of background PAHs in the Peace-Athabasca Delta (Alberta, Canada) using molecular level radiocarbon analysis. Environ. Sci. Technol. 49, 9056–9063.
Jeong, C.H., Hopke, P.K., Kim, E., Lee, D.W., 2004. The comparison between thermal-optical transmittance elemental carbon and Aethalometer black carbon measured at multiple monitoring sites. Atmos. Environ. 38, 5193–5204.
Katsoyiannis, A., Sweetman, A.J., Jones, K.C., 2011. PAH molecular diagnostic ratios applied to atmospheric sources: a critical evaluation using two decades of source inventory and air concentration data from the UK. Environ. Sci. Technol. 45, 8897–8906.
Kavouras, I.G., Koutrakis, P., Tsapakis, M., Lagoudaki, E., Stephanou, E.G., Von Baer, D., Oyola, P., 2001. Source apportionment of urban particulate aliphatic and polynuclear aromatic hydrocarbons (PAHs) using multivariate methods. Environ. Sci. Technol. 35, 2288–2294.
Kelly, E.N., Short, J.W., Schindler, D.W., Hodson, P.V., Ma, M., Kwan, A.K., Fortin, B.L., 2009. Oil sands development contributes polycyclic aromatic compounds to the Athabasca River and its tributaries. Proc. Natl. Acad. Sci., USA 106, 22346–22351.
Korosi, J.B., Cooke, C.A., Eickmeyer, D.C., Kimpe, L.E., Blais, J.M., 2016. In-situ bitumen extraction associated with increased petrogenic polycyclic aromatic compounds in lake sediments from the Cold Lake heavy oil fields (Alberta, Canada). Environ. Pollut. 218, 915–922.
Kreider, M.L., Panko, J.M., McAtee, B.L., Sweet, L.I., Finley, B.L., 2010. Physical and chemical characterization of tire-related particles: comparison of particles generated using different methodologies. Sci. Total Environ. 408, 652–659.
Kurek, J., Kirk, J.L., Muir, D.C.G., Wang, X., Evans, M.S., Smol, J.P., 2013. Legacy of a half century of Athabasca oil sands development recorded by lake ecosystems. Proc. Natl. Acad. Sci. U. S. A. 110, 1761–1766.
Landis, M.S., Pancras, J.P., Graney, J.R., Stevens, R.K., Percy, K.E., Krupa, S., 2012. Receptor modeling of epiphytic lichens to elucidate the sources and spatial distribution of inorganic air pollution in the Athabasca Oil Sands Region. In: Percy, Kevin (Ed.), Alberta Oil Sands: Energy, Industry and the Environment. Elsevier, Oxford, England, pp. 427–467.
Landis, M.S., Pancras, J.P., Graney, J.R., White, E.M., Edgerton, E.S., Legge, A., Percy, K.E., 2017. Source apportionment of ambient fine and coarse particulate matter at the Fort McKay community site, in the Athabasca Oil Sands Region, Alberta, Canada. Sci. Total Environ. 584-585, 105–117.
Landis, M.S., Kamal, A.S., Edgerton, E.S., Wentworth, G., Sullivan, A.P., Dillner, A.M., 2018. The impact of the 2016 Fort McMurray Horse River wildfire on ambient air pollution levels in the Athabasca Oil Sands Region, Alberta, Canada. Sci. Total Environ. 618, 1665–1676.
Landis, M.S., Studabaker, W.B., Pancras, J.P., Graney, J.R., Puckett, K., White, E.M., Edgerton, E.S., 2019. Source apportionment of an epiphytic lichen biomonitor to elucidate the sources and spatial distribution of polycyclic aromatic hydrocarbons in the Athabasca Oil Sands Region, Alberta, Canada. Sci. Total Environ. 654, 1241–1257.
Lundin, J.I., Riffell, J.A., Wasser, S.K., 2015. Polycyclic aromatic hydrocarbons in caribou, moose, and wolf scat samples from three areas of the Alberta oil sands. Environ. Pollut. 206, 527–534.
Makkonen, U., Hellen, H., Anttila, P., Ferm, M., 2010. Size distribution and chemical composition of airborne particles in south-eastern Finland during different seasons and wildfire episodes in 2006. Sci. Total Environ. 408, 644–651.
Manzano, C.A., Marvin, C., Muir, D., Harner, T., Martin, J., Zhang, Y.F., 2017. Heterocyclic aromatics in petroleum coke, snow, lake sediments, and air samples from the Athabasca Oil Sands Region. Environ. Sci. Technol. 51, 5445–5453.
Osacky, M., Geramian, M., Ivey, D.G., Liu, Q., Etsell, T.H., 2013. Mineralogical and chemical composition of petrologic end members of Alberta Oil Sands. Fuel 113, 148–157.
Paatero, P., 1997. Least squares formulation of robust nonnegative factor analysis. Atmos. Environ. 37, 23–35.
Paatero, P., 1999. The multilinear engine - a table-driven least squares program for solving multilinear problems, including the n-way parallel factor analysis model. J. Comput. Graph. Stat. 8, 854–888.
Paatero, P., Tapper, U., 1993. Analysis of different modes of factor analysis as least squares fit problem. Chemom. Intell. Lab. Syst. 18, 183–194.
Pancras, J.P., Landis, M.S., Norris, G.A., Vedantham, R., Dvonch, J.T., 2013. Source apportionment of ambient fine particulate matter in Detroit, Michigan, using hourly resolved PM chemical composition data. Sci. Total Environ. 448, 2–13.
Phillips-Smith, C., Jeong, C.H., Healy, R.M., Zlotorzynska, E.D., Celo, V., Brook, J.R., Evans, G., 2017. Sources of particulate matter components in the Athabasca Oil Sands Region: investigation through a comparison of trace element measurement methodologies. Atmos. Chem. Phys. 17, 9435–9449.
Pleil, J.D., Vette, A.F., Rappaport, S.M., 2004. Assaying particle-bound polycyclic aromatic hydrocarbons from archived $PM_{2.5}$ filters. J. Chromatogr. A 1033, 9–17.
Ramdahl, T., 1983. Retene – a molecular marker of wood combustion in ambient air. Nature 306, 580–582.
Ravindra, K., Sokhi, R., Van Grieken, R., 2008. Atmospheric polycyclic aromatic hydrocarbons: source attribution, emission factors and regulation. Atmos. Environ. 42, 2895–2921.
Reff, A., Eberly, S.I., Bhave, P.V., 2007. Receptor modeling of ambient particulate matter data using positive matrix factorization: review of existing methods. J. Air Waste Manag. Assoc. 57, 146–154.
Sandradewi, Prevot, A.S.H., Szidat, S., Perron, N., Alfarra, M.R., Lanz, V.A., Weingartner, E., Baltensperger, W., 2008. Using aerosol light absorption measurements for the quantitative determination of wood burning and traffic emission contributions to particulate matter. Environ. Sci. Technol. 42, 3316–3323.
Schauer, J.J., Rogge, W.F., Hildemann, L.M., Mazurek, M.A., Cass, G.R., 1996. Source apportionment of airborne particulate matter using organic compounds as tracers. Atmos. Environ. 30, 3837–3855.
Schindler, D.W., 2014. Unravelling the complexity of pollution by the oil sands industry. Proc. Natl. Acad. Sci. U. S. A. 111, 3209–3210.
Schuster, J.K., Harner, T., Su, K., Mihele, C., Eng, A., 2015. First results from the oil sands passive air monitoring network for polycyclic aromatic compounds. Environ. Sci. Technol. 49, 2991–2998.
Simoneit, B.R.T., 2002. Biomass burning – a review of organic tracers for smoke from incomplete combustion. Appl. Geochem. 17, 129–162.
Stogiannidis, E., Laane, R., 2015. Source characterization of polycyclic aromatic hydrocarbons by using their molecular indices: an overview of possibilities. In: Whitacre, D. (Ed.), Reviews of Environmental Contamination and Toxicology (Continuation of Residue Reviews). 234. Springer, Cham.
Stracquadanio, M., Trombini, C., 2006a. Gas to particle (PM10) partitioning of polycyclic aromatic hydrocarbons (PAHs) in a typical urban environment of the Po Valley (Bologna, Italy). Fresenius Environ. Bull. 15, 1276–1286.
Stracquadanio, M., Trombini, C., 2006b. Particulate matter, gas-phase and particle-bound polycyclic aromatic hydrocarbons in an urban environment heavily impacted by vehicular traffic (Bologna, Italy). Ann. Chim. 96, 463–478.
Studabaker, W., Puckett, K.J., Percy, K.E., Landis, M.S., 2017. Determination of polynuclear aromatic hydrocarbons, dibenzothiophene, and alkylated homologs in the lichen Hypogymnia physodes by gas chromatography using single quadrupole mass spectroscopy and time-of-flight mass spectroscopy. Chromatography A 1492, 106–116.
U.S. Environmental Protection Agency, January 1999. Compendium of methods for the determination of toxic organic compounds in ambient air second edition, Compendium method TO-13A, determination of polycyclic aromatic hydrocarbons (PAHs) in ambient air using Gas Chromatography/Mass Spectrometry (GC/MS). Office of Research and Development, Cincinnati, OH, USA EPA/625/R-96/010b. https://www3.epa.gov/ttnamti1/files/ambient/airtox/to-13arr.pdf, Accessed date: 16 February 2019.
U.S. Environmental Protection Agency, April 2014. EPA Positive Matrix Factorization (PMF) 5.0 Fundamentals & User Guide. Report No. EPA-600/R-14/108. Office of Research and Development, Washington, DC, USA.
Vedantham, R., Norris, G., Brown, S.G., Roberts, P., 2012. Combining continuous near-road monitoring and inverse modeling to isolate the effect of highway expansion on a school in Las Vegas. Atmos. Pollut. Res. 3, 105–111.
Venter, A.D., Van Zyl, P.G., Beukes, J.P., Josipovic, M., Hendriks, J., Vakkari, V., Laakso, L., 2016. Atmospheric trace metals measured at a regional background site 920 (Welgegund) in South Africa. Atmos. Chem. Phys. 17, 4251–4263.
Wang, Z.D., Fingas, M.F., 2003. Development of oil hydrocarbon fingerprinting and identification techniques. Mar. Pollut. Bull. 47 (9–12), 423–452.
Wang, Z.D., Fingas, M., Shu, Y.Y., Sigouin, L., Landriault, M., Lambert, P., Turpin, R., Campagna, P., Mullin, J., 1999. Quantitative characterization of PAHs in burn residue

and soot samples and differentiation of pyrogenic PAHs from petrogenic PAHs - the 1994 Mobile Burn Study. Environ. Sci. Technol. 33, 3100–3109.
Wang, Y., Huang, J., Zananski, T.J., Hopke, P.K., Holsen, T.M., 2010. Impacts of the Canadian forest fires on atmospheric mercury and carbonaceous aerosols in northern New York. Environ. Sci. Technol. 44, 8435–8440.
Wang, Y., Hopke, P.K., Rattigan, O.V., Xia, X., Chalupa, D.C., Utell, M.J., 2011a. Characterization of residential wood combustion particles using the two-wavelength Aethalometer. Environ. Sci. Technol. 45, 7387–7393.
Wang, Y., Hopke, P.K., Rattigan, O.V., Zhu, Y., 2011b. Characterization of ambient black carbon and wood burning particles in two urban areas. J. Environ. Monit. 13, 1919–1926.
Wang, Z.D., Yang, C., Parrott, J.L., Frank, R.A., Yang, Z., Brown, C.E., Hollebone, B.P., Landriault, M., Fieldhouse, B., Liu, Y., Zhang, G., Hewitt, L.M., 2014. Forensic source differentiation of petrogenic, pyrogenic, and biogenic hydrocarbons in Canadian oil sands environmental samples. J. Hazard. Mater. 271, 166–177.
Wang, X., Chow, J.C., Kohl, S.D., Percy, K.E., Legge, A.H., Watson, J.G., 2015. Characterization of $PM_{2.5}$ and PM_{10} fugitive dust source profiles in the Athabasca Oil Sands Region. J. Air Waste Manage. Assoc. 65, 1421–1433.
Wang, X., Chow, J.C., Kohl, S.D., Percy, K.E., Legge, A.H., Watson, J.G., 2016. Real-world emission factors for Caterpillar 797B heavy haulers during mining operations. Particuology 28, 22–30.
Wentworth, G., Aklilu, Y.A., Landis, M.S., Hsu, Y.M., 2018. Impacts of a large boreal wildfire on ground level atmospheric concentrations of PAHs, VOCs and ozone. Atmos. Environ. 178, 19–30.
Wik, A., Dave, G., 2009. Occurrence and effects of tire wear particles in the environment - a critical review and an initial risk assessment. Environ. Pollut. 157, 1–11.
Wnorowski, A., 2017. Characterization of the ambient air content of parent polycyclic aromatic hydrocarbons in the Fort McKay region (Canada). Chemosphere 174, 371–379.
Wood Buffalo Environmental Association, 2011. Annual report – continuous monitoring. March 10, 2012. http://wbea.org/resources/ambient-air-monitoring-reports/ambient-annual-reports, Accessed date: 1 April 2016.
Yang, C., Wang, Z.D., Yang, Z.Y., Hollebone, B., Brown, C.E., Landriault, M., 2011. Chemical fingerprints of Alberta Oil Sands and related petroleum products. Environ. Forensic 12, 173–188.
Yunker, M.B., Macdonald, R.W., Vingarzan, R., Mitchell, R.H., Goyette, D., Sylvestre, S., 2002. PAHs in the Fraser River basin: a critical appraisal of PAH ratios as indicators of PAH sources and composition. Org. Geochem. 33, 489–515.
Zhang, Y., Shotyk, W., Zaccone, C., Noernberg, T., Pellerier, R., Bicalho, B., Froese, D.G., Davies, L., Martin, J.W., 2016. Airborne petcoke dust is a major source of polycyclic aromatic hydrocarbons in the Athabasca Oil Sands Region. Environ. Sci. Technol. 50, 1711–1720.